
Bidirectional Diffusion Bridge Models

Duc Kieu, Kien Do, Toan Nguyen, Dang Nguyen, Thin Nguyen
Applied Artificial Intelligence Institute (A2I2), Deakin University, Australia
{v.kieu, k.do, k.nguyen, d.nguyen, thin.nguyen}@deakin.edu.au

Abstract

Diffusion bridges have shown potential in paired image-to-image (I2I) translation tasks. However, existing methods are limited by their unidirectional nature, requiring separate models for forward and reverse translations. This not only doubles the computational cost but also restricts their practicality. In this work, we introduce the Bidirectional Diffusion Bridge Model (BDBM), a scalable approach that facilitates bidirectional translation between two coupled distributions using a single network. BDBM leverages the Chapman-Kolmogorov Equation for bridges, enabling it to model data distribution shifts across timesteps in both forward and backward directions by exploiting the interchangeability of the initial and target timesteps within this framework. Notably, when the marginal distribution given endpoints is Gaussian, BDBM’s transition kernels in both directions possess analytical forms, allowing for efficient learning with a single network. We demonstrate the connection between BDBM and existing bridge methods, such as Doob’s h -transform and variational approaches, and highlight its advantages. Extensive experiments on high-resolution I2I translation tasks demonstrate that BDBM not only enables bidirectional translation with minimal additional cost but also outperforms state-of-the-art bridge models. Our source code is available at <https://github.com/kvmduc/BDBM>.

1 Introduction

Diffusion models (DMs) [40, 43, 13] have emerged as a powerful class of generative models, surpassing GANs [11] and VAEs [21] in generating high-quality data [7]. These models learn to transform a Gaussian prior distribution into the data distribution through iterative denoising steps. However, the Gaussian prior assumption in diffusion models limits their application, particularly in image-to-image (I2I) translation [16], where the distributions of the two domains are non-Gaussian.

A straightforward solution is to incorporate an additional condition related to one domain into diffusion models for guidance [6, 35]. This approach often overlooks the marginal distribution of each domain, which may hinder its generalization ability, especially when the two domains are diverse and significantly different. In contrast, methods that construct an ODE flow [25, 29, 1] or a Schrödinger bridge [4, 39, 18] between two domains focus mainly on matching the marginal distributions at the boundaries, neglecting the relationships between samples from the two domains. Consequently, these methods are not well-suited for paired I2I tasks.

To solve the paired I2I problem, recent methods [31, 53] leverage knowledge of the target sample y in the pair (x, y) and utilized Doob’s h -transform [9] to construct a bridge that converges to y . This involves learning either the h function [41] or the score function of the h -transformed SDE [53], both of which depend on y . Other methods [24] extend the unconditional variational framework for diffusion models to a conditional one given y for constructing such bridges, thereby learning a backward transition distribution conditioned on y . Despite their success in capturing the correspondence between x and y , these methods share a common limitation: they can only generate

data in *one direction*, from y to x . For the reverse from x to y , a separate bridge must be trained with x being the target, which doubles computational resources and modeling complexity. We argue that real-world applications would greatly benefit from bidirectional generative models capable of transitioning between two distributions using a single model.

Therefore, we introduce a novel bridge model called **Bidirectional Diffusion Bridge Model (BDBM)** that enables *bidirectional* transitions between two coupled distributions using *only a single network*. Our bridge is built on a framework that highlights the symmetry between forward and backward transitions. By utilizing the Chapman-Kolmogorov Equation (CKE) for conditional Markov processes, we transform the problem of modeling the conditional distribution $p(x_T = y | x_0 = x)$ into modeling the forward transition from $p(x_t | x, y)$ to $p(x_s | x, y)$ - the marginal distributions at times t and s ($0 \leq t < s \leq T$) of a *double conditional Markov process (DCMP)* between two endpoints $x, y \sim p(x, y)$. Given the interchangeability of the two marginal distributions, we can model the conditional distribution $p(x_0 = x | x_T = y)$ simply by learning the backward transition from $p(x_s | x, y)$ to $p(x_t | x, y)$ without altering the DCMP. Notably, the forward and backward transition distributions of the DCMP are connected through Bayes' rule and can be expressed analytically as Gaussian distributions when the DCMP is a diffusion process. This insight motivates us to reparameterize models of the forward and backward transition distributions in a way that they share a common term. Therefore, we can use a single network for modeling this term and train it with a unified objective for both directions.

We evaluate our method on four popular paired I2I translation datasets [16, 49] with image sizes up to 256×256 , considering both pixel and latent spaces. Experimental results demonstrate that BDBM surpasses state-of-the-art (SOTA) unidirectional diffusion bridge models in terms of visual quality (measured by FID) and perceptual similarity (measured by LPIPS) of generated samples, while requiring similar or even fewer training iterations. These promising results showcase the clear advantages of our method, which not only facilitates bidirectional translation at minimal additional cost but also improves performance.

2 Preliminaries

2.1 Markov Processes and Diffusion Processes

A Markov process is a stochastic process satisfying the Markov property, i.e., the future (state) is independent of the past given the present:

$$p(x_s | x_t, x_u) = p(x_s | x_t)$$

where x_u, x_t, x_s denote random states at times u, t, s satisfying that $0 \leq u < t < s$. Here, $p(x_s | x_t)$ is the transition distribution of the Markov process.

Diffusion processes are special cases of Markov processes where the transition distribution is typically a Gaussian distribution. A diffusion process can be either discrete-time [13] or continuous-time [44]. A continuous-time diffusion process can be described by the following (forward) stochastic differential equation (SDE):

$$dX_t = \mu(t, X_t) dt + \sigma(t, X_t) dW_t \quad (1)$$

where W_t denotes the Wiener process (aka Brownian motion) at time t . Eq. 1 can be solved via simulation provided that the distribution of X_0 is known. One can derive the *forward* and *backward Kolmogorov equations* (KFE and KBE) for this SDE as follows:

$$\text{KFE: } \frac{\partial p(t, x)}{\partial t} = \mathcal{G}^* p(t, x); p(0, \cdot) \text{ is given} \quad (2)$$

$$\text{KBE: } \frac{\partial p(T, y | t, x)}{\partial t} = -\mathcal{G} p(T, y | t, x); p(T, \cdot) \text{ is given} \quad (3)$$

where \mathcal{G} denotes the *generator* corresponding to the SDE in Eq. 1 and \mathcal{G}^* is the adjoint of \mathcal{G} . When $\sigma(t, x)$ is a scalar depending only on t (i.e., $\sigma(t, x) \equiv \sigma(t)$, for a real-valued function f , $\mathcal{G}f(t, x)$ and $\mathcal{G}^*f(t, x)$ are given by:

$$\begin{aligned} \mathcal{G}f(t, x) &= \nabla f(t, x)^\top \mu(t, x) + \frac{\sigma(t)^2}{2} \Delta f(t, x) \\ \mathcal{G}^*f(t, x) &= -\nabla \cdot (f(t, x) \mu(t, x)) + \frac{\sigma(t)^2}{2} \Delta f(t, x) \end{aligned}$$

where $\nabla \cdot$ and Δ denote the divergence and Laplacian, respectively.

2.2 Chapman-Kolmogorov Equations

A Markov process can be described via the *Chapman-Kolmogorov equation* (CKE) [17] as follows:

$$p(x_s|x_t) = \int p(x_s|x_r) p(x_r|x_t) dx_r \quad (4)$$

which holds for all times t, r, s satisfying that $0 \leq t < r < s \leq T$. The CKE in Eq. 4 can be considered as the integral form of the KFE and KBE in Eqs. 2, 3. Compared to the Kolmogorov equations, the CKE is easier to work with since (i) it does not involve the partial derivatives of the transition kernel, (ii) it is applicable to both continuous- and discrete-time Markov processes, and (iii) it encapsulates both forward and backward transitions. Regarding the last point, we can apply Eq. 4 either in the forward manner (from 0 to T) to evaluate the distribution of the next state x_s given the distribution of the current state x_t :

$$p(x_s|x_0) = \int p(x_s|x_t) p(x_t|x_0) dx_t; p(x_t|x_0) \text{ is given} \quad (5)$$

or in the backward manner (from T to 0) to evaluate the distribution of the previous state x_t given the distribution of current state x_s :

$$p(x_T|x_t) = \int p(x_T|x_s) p(x_s|x_t) dx_s; p(x_T|x_s) \text{ is given} \quad (6)$$

In the discrete-time setting, Eq. 5 can be interpreted as given a Markov process with $p(x_{t+1}|x_t)$ specified for every time t . If we have known the marginal distribution $p(x_t|x_0)$ at time t , then by solving the CKE forwardly, we can compute $p(x_{t+1}|x_0)$ at time $t+1$. Similarly, in Eq. 6, if we have known $p(x_T|x_{t+1})$ at time $t+1$, then by solving the CKE backwardly, we can compute $p(x_T|x_t)$ at time t . For example, in DDPM [13], given $p(x_t|x_0) = \mathcal{N}(x_t | \sqrt{\bar{\alpha}_t}x_0, (1 - \bar{\alpha}_t)\mathbf{I})$ and $p(x_{t+1}|x_t) = \mathcal{N}(x_{t+1} | \sqrt{1 - \beta_{t+1}}x_t, \beta_{t+1}\mathbf{I})$, we can use Eq. 5 to compute $p(x_{t+1}|x_0)$ as $\mathcal{N}(x_{t+1} | \sqrt{\bar{\alpha}_{t+1}}x_0, (1 - \bar{\alpha}_{t+1})\mathbf{I})$.

Interestingly, the backward CKE in Eq. 6 can be written in another way according to Bayes' rule:

$$p(x_t|x_T) = \int p(x_t|x_s) p(x_s|x_T) dx_s; p(x_s|x_T) \text{ is given} \quad (7)$$

The mathematical derivation is detailed in Appdx. A.1. Eq. 7 is akin to the forward CKE in Eq. 5 but in reverse time.

3 Method

3.1 Chapman-Kolmogorov Equations for Bridges

In many real-world problems (e.g., paired/unpaired image translation), the joint boundary distribution $p(y_A, y_B)$ of samples from two domains A, B is given in advance rather than just either $p(y_A)$ or $p(y_B)$, and we need to design a stochastic process such that if we start from y_A (y_B), we should reach y_B (y_A) with a predefined probability $p(y_B|y_A)$ ($p(y_A|y_B)$). Such stochastic processes are referred to as *stochastic bridges* or simply *bridges* [30, 31, 24, 53]. In this section, we will develop mathematical models for stochastic bridges based on the CKEs for Markov processes in Section 2.

Without loss of generality, we associate two domains A, B with samples at time 0, T , respectively. Let $\{X_t\}$ be a stochastic process in which the initial distribution $p(x_0|y_A)$ is a Dirac distribution at y_A (i.e., $p(x_0|y_A) = \delta_{y_A}$). To conform to the notation used in prior works, we denote $\hat{x}_0 := y_A$. The symbol $\hat{\cdot}$ indicates that \hat{x}_0 is a specified value rather than a random state like x_0 ¹. For modeling

¹This allows us to write $p(x_0|\hat{x}_0) = \delta_{\hat{x}_0} = \delta_{y_A}$

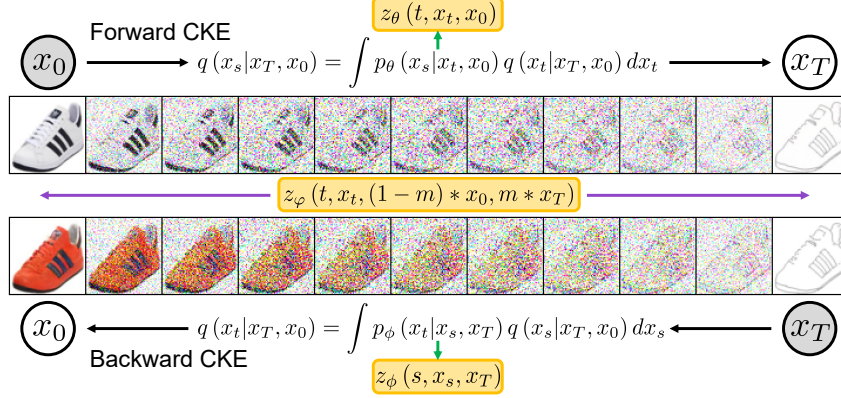


Figure 1: An illustration of *Bidirectional Diffusion Bridge Models (BDBM)*. Instead of learning two separate models $z_\theta(t, x_t, x_0)$ and $z_\phi(s, x_s, x_T)$ for the forward and backward transitions, we learn a single model $z_\varphi(t, x_t, (1-m)*x_0, m*x_T)$ with a binary mask m that enables transition in both directions. Grey and white nodes denote initial and generated samples, respectively.

simplicity, we assume that the process is a *conditional Markov process* described by the following CKE:

$$p(x_v|x_t, \hat{x}_0) = \int p(x_v|x_s, \hat{x}_0) p(x_s|x_t, \hat{x}_0) dx_s \quad (8)$$

where $t < s < v$. Interestingly, if we start this process from an arbitrary time t with the marginal distribution $p(x_t|\hat{x}_0)$, we will always reach the same distribution at time $T > t$. To see this, we represent $p(x_T|\hat{x}_0)$ using two different starting times t, s with $0 \leq t < s < T$ as follows:

$$\begin{aligned} & p(x_T|\hat{x}_0) \\ &= \int p(x_T|x_s, \hat{x}_0) p(x_s|\hat{x}_0) dx_s \end{aligned} \quad (9)$$

$$= \int p(x_T|x_s, \hat{x}_0) \left(\int p(x_s|x_t, \hat{x}_0) p(x_t|\hat{x}_0) dx_t \right) dx_s \quad (10)$$

$$= \int \underbrace{\left(\int p(x_T|x_s, \hat{x}_0) p(x_s|x_t, \hat{x}_0) dx_s \right)}_{p(x_T|x_t, \hat{x}_0)} p(x_t|\hat{x}_0) dx_t \quad (11)$$

$$= \int p(x_T|x_t, \hat{x}_0) p(x_t|\hat{x}_0) dx_t \quad (12)$$

The intuition here is the associativity of the (functional) inner product between $p(x_T|x_s, \hat{x}_0)$, $p(x_s|x_t, \hat{x}_0)$, and $p(x_t|\hat{x}_0)$. Let us consider the problem of learning the transition kernel $p_\theta(x_s|x_t, \hat{x}_0)$ of the above process such that $p_\theta(x_T|\hat{x}_0)$ equals $p(y_B|y_A)$. Clearly, $p_\theta(x_s|x_t, \hat{x}_0)$ should satisfy:

$$p(x_T|x_t, \hat{x}_0) = \int p(x_T|x_s, \hat{x}_0) p_\theta(x_s|x_t, \hat{x}_0) dx_s \quad (13)$$

for all $0 \leq t < s$. However, Eq. 13 does not facilitate easy learning of $p_\theta(x_s|x_t, \hat{x}_0)$ because determining the values of $p(x_T|x_t, \hat{x}_0)$ and $p(x_T|x_s, \hat{x}_0)$ can be challenging in practice, which usually requires another parameterized model. Therefore, we utilize the equivalent formula below:

$$q(x_s|\hat{x}_T, \hat{x}_0) = \int p_\theta(x_s|x_t, \hat{x}_0) q(x_t|\hat{x}_T, \hat{x}_0) dx_t \quad (14)$$

with $\hat{x}_T \sim p(y_B|y_A)$. The derivation of Eq. 14 is presented in Appdx. A.2. Eq. 14 implies that if we can construct a *double conditional Markov process* between \hat{x}_0 and \hat{x}_T such that the marginal distribution at time t is $q(x_t|\hat{x}_T, \hat{x}_0)$ and the two boundary distributions at times 0 and T are Dirac distributions at \hat{x}_0 and \hat{x}_T , respectively (i.e., $q(x_0|\hat{x}_T, \hat{x}_0) = \delta_{\hat{x}_0}(x_0)$ and $q(x_T|\hat{x}_T, \hat{x}_0) = \delta_{\hat{x}_T}(x_T)$), then by learning $p_\theta(x_s|x_t, \hat{x}_0)$ to match the transition probability $q(x_s|x_t, \hat{x}_T, \hat{x}_0)$ of this process, $p_\theta(x_s|x_t, \hat{x}_0)$ will serve as the transition probability of a bridge starting from \hat{x}_0

and ending at \hat{x}_T with $p(\hat{x}_T|\hat{x}_0) = p(y_B|y_A)$. There are various ways to align $p_\theta(x_s|x_t, \hat{x}_0)$ with $q(x_s|x_t, \hat{x}_T, \hat{x}_0)$ and the loss below is commonly used due to its link to variational inference [13, 24]:

$$\mathcal{L} = \mathbb{E}_{t,s,\hat{x}_0,\hat{x}_T} [D_{\text{KL}}(q(x_s|x_t, \hat{x}_T, \hat{x}_0) \| p_\theta(x_s|x_t, \hat{x}_0))] \quad (15)$$

where $t \sim \mathcal{U}(0, T - \Delta t)$, $s = t + \Delta t$, $\hat{x}_0 \sim p(y_A)$, $\hat{x}_T \sim p(y_B|y_A)$.

In practice, we often choose $q(x_t|\hat{x}_T, \hat{x}_0)$ and $q(x_s|\hat{x}_T, \hat{x}_0)$ to be Gaussian distributions, which results in $q(x_s|x_t, \hat{x}_T, \hat{x}_0)$ being a Gaussian. Therefore, if $p_\theta(x_s|x_t, \hat{x}_0)$ is also modeled as a Gaussian distribution, then Eq. 15 can be expressed in closed-form. Details about this will be presented in Section 3.2. In Appdx. A.4, we provide the connection of this framework to variational inference, score matching, and Doob’s h -transform.

3.2 Generalized Diffusion Bridge Models

To simplify our notation, from this section onward, we will use x_0, x_T in place of \hat{x}_0, \hat{x}_T in the conditional distributions $q(x_t|\hat{x}_0, \hat{x}_T)$ and $q(x_s|x_t, \hat{x}_0, \hat{x}_T)$ with a note that they should be interpreted as specified values rather than random states. As discussed in Section 3.1, $q(x_t|x_0, x_T)$ should be chosen as a Gaussian distribution with zero variance at $t \in \{0, T\}$ to facilitate learning the transition kernel. A general formula of $q(x_t|x_0, x_T)$ is $q(x_t|x_0, x_T) = \mathcal{N}(\alpha_t x_0 + \beta_t x_T, \sigma_t^2 \mathbf{I})$ where $\alpha_t, \beta_t, \sigma_t$ are continuously differentiable functions of $t \in [0, T]$ satisfying $\alpha_0 = \beta_T = 1$ and $\alpha_T = \beta_0 = \sigma_0 = \sigma_T = 0$. According to this formula, $x_t \sim q(x_t|x_0, x_T)$ can be computed as follows:

$$x_t = \alpha_t x_0 + \beta_t x_T + \sigma_t z \quad (16)$$

with $z \sim \mathcal{N}(0, \mathbf{I})$. Similarly, we have $q(x_s|x_0, x_T) = \mathcal{N}(\alpha_s x_0 + \beta_s x_T, \sigma_s^2 \mathbf{I})$. This means $q(x_s|x_t, x_0, x_T)$ has the form $\mathcal{N}(x_s | \mu(s, t, x_t, x_0, x_T), \delta_{s,t}^2 \mathbf{I})$ where:

$$\begin{aligned} & \mu(s, t, x_t, x_0, x_T) \\ &= \alpha_s x_0 + \beta_s x_T + \sqrt{\sigma_s^2 - \delta_{s,t}^2} \frac{(x_t - \alpha_t x_0 - \beta_t x_T)}{\sigma_t} \end{aligned} \quad (17)$$

$$= \frac{\beta_s}{\beta_t} x_t + \left(\alpha_s - \alpha_t \frac{\beta_s}{\beta_t} \right) x_0 + \left(\sqrt{\sigma_s^2 - \delta_{s,t}^2} - \sigma_t \frac{\beta_s}{\beta_t} \right) z \quad (18)$$

and $\delta_{s,t}$ can vary arbitrarily within the (half-)interval $[0, \sigma_s)$. Eq. 18 is derived from Eq. 17 by setting $x_T = \frac{1}{\beta_t} (x_t - \alpha_t x_0 - \sigma_t z)$ according to Eq. 16.

To match $p_\theta(x_s|x_t, x_0)$ with $q(x_s|x_t, x_0, x_T)$ ($t < s$), we should be able to infer x_T from x_t, x_0 in $p_\theta(x_s|x_t, x_0)$. A straightforward approach is to formulate $p_\theta(x_s|x_t, x_0)$ as $\mathcal{N}(x_s | \mu_\theta(s, t, x_t, x_0), \delta_{s,t}^2 \mathbf{I})$ and reparameterize $\mu_\theta(s, t, x_t, x_0)$ to match with $\mu(s, t, x_t, x_0, x_T)$, where x_T replaced by its approximation $x_{T,\theta}(t, x_t, x_0)$ in Eq. 17 (or z replaced by $z_\theta(t, x_t, x_0)$ in Eq. 18). When $z_\theta(t, x_t, x_0)$ is modeled, we regard $x_{T,\theta}(t, x_t, x_0)$ as $\frac{1}{\beta_t} (x_t - \alpha_t x_0 - \sigma_t z_\theta(t, x_t, x_0))$, and the loss in Eq. 15 simplifies to:

$$\mathcal{L} = \mathbb{E}_{t,x_0,x_T,z,x_t} \left[w_t \|z_\theta(t, x_t, x_0) - z\|_2^2 \right] \quad (19)$$

where $t \sim \mathcal{U}(0, T)$, $x_0 \sim p(y_A)$, $x_T \sim p(y_B|y_A)$, $z \sim \mathcal{N}(0, \mathbf{I})$, and $x_t = \alpha_t x_0 + \beta_t x_T + \sigma_t z$. w_t is set to 1 in our work. This loss is a weighted version of the score matching loss for bridges [53]. Once z_θ has been learned, it will approximate $-\sigma_t \nabla \log p(x_t|x_0)$, and $x_{T,\theta}$ derived from z_θ approximates $\mathbb{E}_{p(x_T|x_t, x_0)} [x_T]$ due to Tweedie’s formula for bridges (Appdx. A.3).

3.3 Bidirectional Diffusion Bridge Models

Learning $p_\theta(x_s|x_t, x_0)$ with $t < s$ in Section 3.2 leads to a bridge that maps samples at time 0 (domain A) to those at time T (domain B). Unfortunately, we cannot travel in the reverse direction (i.e., generate x_0 from x_T) with this bridge. It is because the reverse transition kernel derived from $p_\theta(x_s|x_t, x_0)$ requires the knowledge of x_0 , which is not available if starting from time T . A straightforward solution to this problem is constructing another bridge with x_T as the source by learning $p_\phi(x_t|x_s, x_T)$ ($t < s$). This results in two separate models for forward and backward travels, which doubles the resources for training and deployment. To overcome this limitation, we propose a

| Model | Edges→Shoes×64 | | | Edges→Handbags×64 | | | Normal→Outdoor×256 | | |
|-------------------|----------------|-------------|-------------|-------------------|-------------|-------------|--------------------|-------------|-------------|
| | FID ↓ | IS ↑ | LPIPS ↓ | FID ↓ | IS ↑ | LPIPS ↓ | FID ↓ | IS ↑ | LPIPS ↓ |
| BBDM | 2.11 | 3.23 | <u>0.05</u> | 6.38 | 3.71 | 0.19 | 8.79 | 5.48 | 0.29 |
| I ² SB | 2.14 | 3.41 | 0.06 | 6.05 | <u>3.73</u> | 0.17 | <u>5.48</u> | 5.71 | 0.37 |
| DDBM | 6.42 | 3.26 | 0.12 | 3.89 | 3.58 | 0.23 | 6.16 | 5.74 | 0.35 |
| BDBM-1 (ours) | <u>1.78</u> | <u>3.28</u> | 0.07 | <u>3.83</u> | 3.71 | <u>0.11</u> | 7.17 | 5.97 | 0.11 |
| BDBM (ours) | 1.06 | <u>3.28</u> | 0.02 | 3.06 | 3.74 | 0.08 | 4.67 | <u>5.91</u> | <u>0.16</u> |

Table 1: Quantitative comparison between BDBM and unidirectional bridge models on translation tasks from sketch/normal maps to color images. The best results are highlighted in bold, while the second-best results are underlined.

novel Bidirectional Diffusion Bridge Model (BDBM) that enables bidirectional travel while requiring the training of only a single network. In our model, $p_\theta(x_s|x_t, x_0)$ and $p_\phi(x_t|x_s, x_T)$ are transition kernels operating in opposite directions along the same bridge that connects x_0 and x_T . Due to the interchangeability between x_t and x_s in Eq. 14, it follows that if $p_\theta(x_s|x_t, x_0)$ approximates $q(x_s|x_t, x_0, x_T)$, then $p_\phi(x_t|x_s, x_T)$ should approximate $q(x_t|x_s, x_0, x_T)$, which is derived from $q(x_s|x_t, x_0, x_T)$ via the Bayes’ rule:

$$q(x_t|x_s, x_0, x_T) = q(x_s|x_t, x_0, x_T) \frac{q(x_t|x_0, x_T)}{q(x_s|x_0, x_T)} \quad (20)$$

Since $q(x_t|x_0, x_T)$, $q(x_s|x_0, x_T)$, and $q(x_s|x_t, x_0, x_T)$ are Gaussian distributions specified in Eqs. 16, 17, $q(x_t|x_s, x_0, x_T)$ is also a Gaussian distribution of the form $\mathcal{N}(x_t | \tilde{\mu}(t, s, x_s, x_0, x_T), \frac{\delta_{s,t}^2 \sigma_t^2}{\sigma_s^2} \mathbf{I})$ with $\tilde{\mu}(t, s, x_s, x_0, x_T)$ given by:

$$\begin{aligned} & \tilde{\mu}(t, s, x_s, x_0, x_T) \\ &= \alpha_t x_0 + \beta_t x_T + \sigma_t \sqrt{\sigma_s^2 - \delta_{s,t}^2} \frac{(x_s - \alpha_s x_0 - \beta_s x_T)}{\sigma_s^2} \end{aligned} \quad (21)$$

$$= \frac{\alpha_t}{\alpha_s} x_s + \left(\beta_t - \beta_s \frac{\alpha_t}{\alpha_s} \right) x_T + \left(\frac{\sigma_t \sqrt{\sigma_s^2 - \delta_{s,t}^2}}{\sigma_s} - \sigma_s \frac{\alpha_t}{\alpha_s} \right) z' \quad (22)$$

where Eq. 22 is derived from Eq. 21 by setting $x_0 = \frac{1}{\alpha_s} (x_s - \beta_s x_T - \sigma_s z')$. We can align $p_\phi(x_t|x_s, x_T)$ with $q(x_t|x_s, x_0, x_T)$ by reparameterizing the mean $\tilde{\mu}_\phi(t, s, x_s, x_T)$ of $p_\phi(x_t|x_s, x_T)$ such that it has the same formula as $\tilde{\mu}(t, s, x_s, x_0, x_T)$ in Eq. 21 but with x_0 replaced by $x_{0,\phi}(s, x_s, x_T)$ (or z' replaced by $z_\phi(s, x_s, x_T)$ in Eq. 22).

In the case where $p_\theta(x_s|x_t, x_0)$ and $p_\phi(x_t|x_s, x_T)$ are modeled via $z_\theta(t, x_t, x_0)$ and $z_\phi(s, x_s, x_T)$, respectively, it is possible to use a single network z_φ instead of two separate networks z_θ and z_ϕ because they both represent the same noise variable $z \sim \mathcal{N}(0, \mathbf{I})$ (given $t = s$). To deal with the problem that the forward transition depends on x_0 while the backward transition depends on x_T , we feed both x_0 and x_T as inputs to z_φ and mask one of them using a mask m associated with the transition direction. This results in the model $z_\varphi(t, x_t, (1-m)*x_0, m*x_T)$ where $m = 0$ (1) if we move forward from 0 to T (backward from T to 0). We learn z_φ by minimizing the following loss:

$$\mathcal{L}_{\text{BDBM}} = \mathbb{E}_{t, x_0, x_T, z, x_t, m} \left[w_t \| z_\varphi(t, x_t, (1-m)*x_0, m*x_T) - z \|_2^2 \right] \quad (23)$$

where x_0, x_T, t, z, x_t are sampled in the same way as in Eq. 19, and the mask m is sampled from the Bernoulli distribution with $p(m = 1) = 0.5$.

On the other hand, when $x_{T,\theta}(t, x_t, x_0)$ and $x_{0,\phi}(s, x_s, x_T)$ serve as the parameterized models for $p_\theta(x_s|x_t, x_0)$ and $p_\phi(x_t|x_s, x_T)$, respectively, we propose to use a unified model to predict $x_0 + x_T$. We denote this model as $s_\varphi(t, x_t, (1-m)*x_0, m*x_T)$ and learn it with the loss:

$$\mathcal{L}_{\text{BDBM}}^{(2)} = \mathbb{E}_{t, x_0, x_T, z, x_t, m} \left[w_t \| s_\varphi(t, x_t, (1-m)*x_0, m*x_T) - (x_0 + x_T) \|_2^2 \right] \quad (24)$$

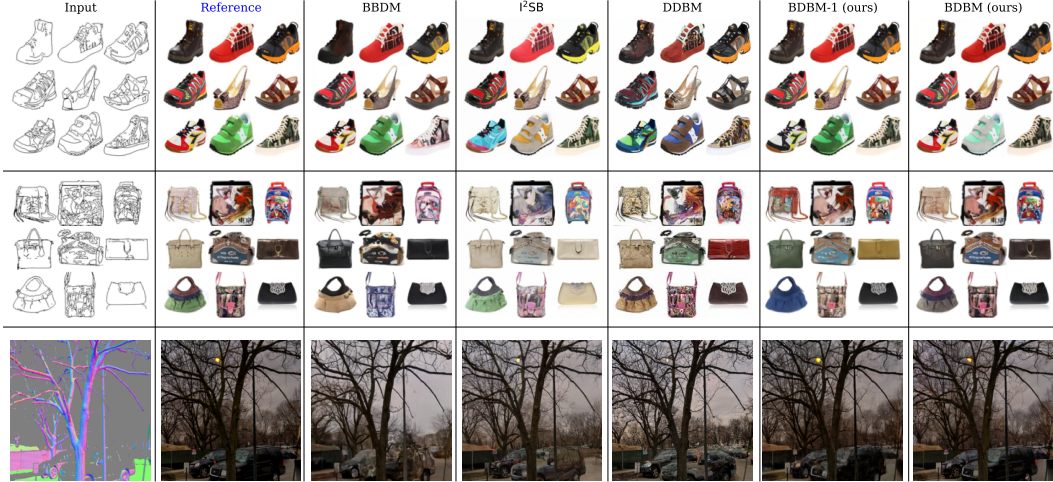


Figure 2: Images generated by BDBM and unidirectional baselines in the Edges→Shoes, Edges→Handbags, and Normal→Outdoor translation tasks.

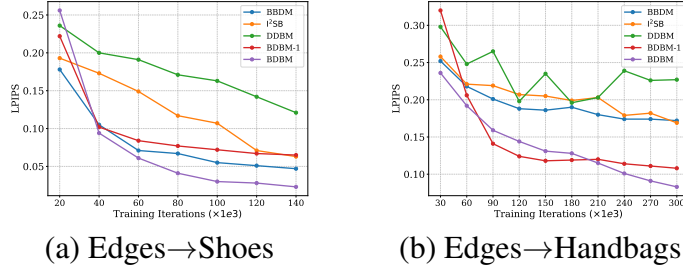


Figure 3: LPIPS curves of BDBM and unidirectional baselines on Edges→Shoes and Edges→Handbags.

When traveling from 0 to T (from T to 0), we set m to 0 (1) and use $s_\varphi(t, x_t, x_0, 0) - x_0$ ($s_\varphi(s, x_s, 0, x_T) - x_T$) to mimic $x_{T,\theta}(t, x_t, x_0)$ ($x_{0,\phi}(s, x_s, x_T)$). We can also train s_φ to predict $x_0 + x_T$. In Appdx. A.7, we provide detailed training and sampling algorithms for BDBM. We also discuss several important variants of BDBM in Appdx. A.6.

4 Experiments

4.1 Experimental Settings

4.1.1 Datasets and evaluation metrics

We validate our method on 4 paired image-to-image (I2I) translation datasets namely Edges↔Shoes, Edges↔Handbags, DIODE Outdoor [49], and Night↔Day [16]. Following [53], we rescale images to 64×64 resolution for the first two datasets and 256×256 for the latter two. We construct bridges in the pixel space for the first three datasets and in the latent space of dimensions $32 \times 32 \times 4$ for the Night↔Day dataset. To map images to latent representations, we use a pretrained VQ-GAN encoder [34]. Following prior work [24], we use FID [12], IS [36], and LPIPS [51] to measure the fidelity and perceptual faithfulness of generated images. These metrics are computed on training samples, as in [53].

4.1.2 Model and training configurations

Unless stated otherwise, we use Brownian bridges, as described in Appdx. A.6.4, with $\alpha_t = 1 - \frac{t}{T}$, $\beta_t = \frac{t}{T}$ and $\sigma_t^2 = k \frac{t}{T} (1 - \frac{t}{T})$ for our experiments. We consider discrete-time models with

| Model | Edges↔Shoes×64 | | | Edges↔Handbags×64 | | |
|-------------|------------------|-------------------|------------------|-------------------|-------------------|------------------|
| | FID ↓ | IS ↑ | LPIPS ↓ | FID ↓ | IS ↑ | LPIPS ↓ |
| DDIB | 85.24/45.19 | 2.13/ 3.40 | 0.38/0.45 | 77.95/31.50 | 2.81/3.59 | 0.49/0.52 |
| RF | 8.63/43.17 | 2.21 /2.79 | 0.03/0.16 | 5.98/48.53 | 3.19 /3.71 | 0.07/0.25 |
| BDBM (ours) | 0.98/1.06 | 2.20/3.28 | 0.01/0.02 | 1.87/3.06 | 3.10/ 3.74 | 0.02/0.08 |

Table 2: Results of BDBM and bidirectional baselines on bidirectional translation tasks. For each method and metric, we report two numbers, the left is for color-to-sketch translation, and the right is for sketch-to-color translation. The best results are highlighted in bold.

$T = 1000$, $\Delta t = 1$, and $k = 2$. Comparison with the continuous-time counterpart is provided in Appdx. B.3. For generation, we employ ancestral sampling with number of function evaluations (NFE) being 200. The variance of the transition kernel $\delta_{s,t}^2$ is set to $\delta_{s,t}^2 = \eta \left(\sigma_s^2 - \sigma_t^2 \frac{\alpha_s^2}{\alpha_t^2} \right)$ with $\eta = 1$. Studies on different values of k and η are presented in Sections 4.3.2, 4.3.3, respectively. We model $z_\varphi(t, x_t, (1-m) * x_0, m * x_T)$ using UNets with ADM architectures [7] customized for different input sizes. For 64×64 images, we use 2 residual blocks with 128 base channels. This allows us to train with batch size of 128 for 64×64 images on an H100 80GB GPU. For 256×256 images, we increase the base channels to 256 and train with batch size of 8. For effective training with batch size of 32, we accumulate gradients over 4 update steps. All models were trained for 140k iterations on the Edges↔Shoes dataset and 300k iterations on the other datasets. The reduced iterations for Edges↔Shoes were due to its smaller training set of 50k samples, compared to 130k for Edges↔Handbags, as well as its smaller image sizes compared to DIODE Outdoor and Night↔Day. The Adam optimizer [20] is employed with a learning rate of 1e-4 and β_1 set to 0.9.

4.1.3 Baselines

We compare our method BDBM with both unidirectional and bidirectional I2I translation baselines. The unidirectional baselines include state-of-the-art (SOTA) diffusion bridge models such as I²SB [27], BBDM [24] and DDBM [53]. We also include a unidirectional variant of our method, referred to as BDBM-1, for comparison to highlight the impact of modeling both directions simultaneously. The bidirectional baselines consist of DDIB [45] and Rectified Flow (RF) [29]. The baselines, excluding RF, were trained using their official code repositories. Since the official RF code does not support parallel training, we used the implementation from [22] for parallel training. For all baselines, we use the same architecture, training configurations, and NFE as our method.

4.2 Experimental Results

4.2.1 Unidirectional I2I translation

Following [53], we experiment with the Edges↔Shoes, Edges↔Handbags, and DIODE Outdoor datasets, focusing on translating sketches or normal maps to color images, as this translation is more challenging than the reverse. Results for the reverse translation are provided in Appdx. B.2.

As shown in Table 1 and Fig. 3, BDBM significantly outperforms BDBM-1 and other unidirectional baselines in most metrics and datasets. This improvement is also evident in the superior quality of samples generated by our method compared to the baselines, as displayed in Fig. 2. Notably, BDBM was trained using the same number of iterations as the baselines. This means that the actual number of model updates w.r.t. a specific direction in BDBM is only *half* that of the baselines, as the two endpoints x_0, x_T are sampled with equal probability in the loss $\mathcal{L}_{\text{BDBM}}$ (Eq. 23). This demonstrates the clear advantage of our proposed bidirectional training over the unidirectional counterpart.

We hypothesize that allowing either x_0 or x_T to serve as the condition for the *shared-parameter* noise model z_φ during training enables the optimizer to leverage the endpoint that yields more accurate predictions for effective parameter updates. Intuitively, this endpoint is likely the one closer in time to the input x_t of the noise model. For instance, consider two noise predictions $z_\varphi(t, x_t, x_0)$ and $z_\varphi(t, x_t, x_T)$ for x_t at time t closer to 0 than to T , where x_0 and x_T are chosen with equal probability. Since x_0 generally provides more reliable information about the noise in x_t compared to x_T , the



Figure 4: Images generated by BDBM and bidirectional baselines on Edges↔Shoes and Edges↔Handbags. “Reference” column shows reference images of the two domains.

| Prediction | Edges→Shoes×64 | | | | Edges→Handbags×64 | | | |
|--------------|----------------|------|---------|-------------|-------------------|------|---------|-------------|
| | FID ↓ | IS ↑ | LPIPS ↓ | Diversity ↑ | FID ↓ | IS ↑ | LPIPS ↓ | Diversity ↑ |
| z | 1.06 | 3.28 | 0.02 | 6.90 | 3.06 | 3.74 | 0.08 | 9.01 |
| $x_T + x_0$ | 1.51 | 3.25 | 0.04 | 2.21 | 3.71 | 3.75 | 0.11 | 7.54 |
| (x_T, x_0) | 1.49 | 3.24 | 0.01 | 1.97 | 3.49 | 3.77 | 0.12 | 7.88 |

Table 3: Results of our method w.r.t. different parameterizations.

optimizer tends to prioritize the output of $z_\varphi(t, x_t, x_0)$ when updating the shared parameters φ . This update not only improves the accuracy of $z_\varphi(t, x_t, x_0)$ but also enhances $z_\varphi(t, x_t, x_T)$ due to the shared parameter structure. In contrast, unidirectional training can only use a single endpoint, for example x_T , as the condition, which reduces its effectiveness in learning model parameters at times t far from T . As x_t becomes increasingly different from x_T , the information provided by x_T becomes less useful for accurately predicting the noise in x_t .

4.2.2 Bidirectional I2I translation

We compare BDBM with bidirectional baselines DDIB and RF, presenting quantitative and qualitative results in Table 2 and Fig. 4. BDBM outperforms the two baselines by large margins for translations in both directions. DDIB struggles to maintain pair consistency between boundary samples due to random mapping into shared Gaussian latent samples, resulting in translations that often differ greatly from the ground truth. Meanwhile, RF performs reasonably well for the color-to-sketch translation but poorly for the reverse. This is because different color images can have very similar sketch images. This causes the learned velocity for the sketch-to-color translation to point toward the average of multiple target color images associated with a source sketch image, as evident in Fig. 4.

4.3 Ablation Study

4.3.1 Impacts of different parameterizations

As discussed in Section 3.3, the transition kernel of BDBM can be modeled by predicting the noise z or endpoints (either by predicting $x_0 + x_T$ and inferring the missing endpoint given the known one, or by directly predicting one endpoint given the other). We compare the effectiveness of these approaches on the Edges→Shoes and Edges→Handbags translation tasks, with results shown in Table 3. In addition to FID and LPIPS metrics, we evaluate Diversity [2, 24], which measures the average pixel-wise standard deviation of multiple color images generated from a single sketch on a held-out test set of 200 samples. We observe that predicting noise achieves slightly better FID scores and produces more diverse samples than predicting endpoints. We hypothesize that since x_0, x_T are

| k | Edges→Shoes×64 | | |
|-----|----------------|---------|-------------|
| | FID ↓ | LPIPS ↓ | Diversity ↑ |
| 1 | 2.07 | 0.04 | 4.61 |
| 2 | 1.06 | 0.02 | 6.90 |
| 4 | 2.35 | 0.03 | 7.26 |
| 8 | 3.52 | 0.05 | 7.81 |

Table 4: Results of BDBM on Edges→Shoes w.r.t. different values of k controlling the variance σ_t^2 .

| | | Edges→Shoes×64 | | | | | |
|--------|-----|----------------|------|------|------|------|------|
| | | NFE | 20 | 50 | 100 | 200 | 1000 |
| η | 0.0 | 4.16 | 2.98 | 2.47 | 2.15 | 1.87 | |
| | 0.2 | 3.37 | 2.31 | 1.79 | 1.42 | 1.14 | |
| | 0.5 | 2.63 | 1.69 | 1.38 | 1.10 | 0.96 | |
| | 1.0 | 2.11 | 1.52 | 1.25 | 1.06 | 0.92 | |

Table 5: FID scores of BDBM on Edges→Shoes w.r.t. different values of η controlling the variance $\delta_{s,t}^2$ and different numbers of sampling steps.

fixed while z is sampled randomly during training, predicting endpoints tends to have less variance than predicting noise, which results in less diverse samples.

4.3.2 Effect of the noise variance σ_t^2

In Section 4.1.2, the noise variance σ_t^2 of BDBM is defined as $\sigma_t^2 = k \frac{t}{T} (1 - \frac{t}{T})$, which means we can control σ_t^2 by changing the value of k . Table 4 shows the results on Edges→Shoes for different values of $k \in \{1, 2, 4, 8\}$. Increasing k generally yields more diverse samples but worsens FID and LPIPS scores. This trade-off occurs because higher k values increase the variance of the distribution $q(x_t|x_0, x_T)$, enlarging the path space and consequently making the model optimization more challenging. Conversely, when k is too small, the noise variance becomes insufficient to corrupt domain information for effective translation. Our results indicate that $k = 2$ offers the best balance between diversity and quality.

4.3.3 Effect of the variance $\delta_{s,t}^2$ of the transition kernel

We study the impact of varying the variance $\delta_{s,t}^2$ of the transition kernel via changing η (Section 4.1.2) on generation quality, with the results presented in Table 5 and Fig. 5. We observe that increasing

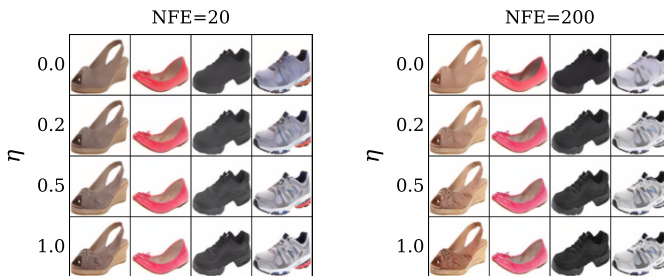


Figure 5: Samples generated by BDBM when translating from sketches to shoes using NFE=20 and NFE=200 for w.r.t. different values of η .

| Model | Day→Night×256 | | |
|--------------------|---------------|-------------|-------------|
| | FID ↓ | IS ↑ | LPIPS ↓ |
| RF | 12.38 | 3.90 | 0.37 |
| DDIB | 226.9 | 2.11 | 0.79 |
| I ² SB | 15.56 | 4.03 | 0.36 |
| DDBM | 27.63 | 3.92 | 0.55 |
| BDBM (ours) | 6.63 | 4.18 | 0.34 |

Table 6: Comparison of BDBM and baseline methods on the Day→Night translation task in latent spaces. Baseline results are sourced from [53]

η from 0 to 1 consistently improves the quality of generated results, regardless of the number of sampling steps. The reason is that the target bridge process connecting boundary points from the two domains is stochastic and corresponds to $\eta = 1$. Consequently, higher η values make x_t more likely to be a sample from the target distribution at time t , leading to better results.

4.3.4 Translation in latent spaces

To validate BDBM’s translation capability in latent spaces, we adopt the Day→Night translation experiment from [53]. For a fair comparison, we maintain the same experimental settings as in [53], including the model architecture, training iterations, and NFE=53 for sample generation. We also follow [53] and compute metrics using the reconstructed versions of the ground-truth target images. This helps mitigate the impact of the VQ-GAN decoding process and ensures that the results accurately reflect the translation quality. Table 6 presents the results of BDBM and baseline methods, with the baseline results taken from [53]. It is evident that BDBM significantly outperforms the baselines, demonstrating its consistent performance in both pixel and latent spaces. We also observed that BDBM effectively captures the statistics of the two domains, where in the dataset, nighttime images are much less diverse than daytime ones, leading to the generation of duplicated nighttime images when using different random seeds, as illustrated in Fig. 8.

5 Related Work

5.1 Schrödinger Bridges and Diffusion Bridges

Recent bridge models can broadly be classified into Schrödinger bridges (SB) and diffusion bridges (DB). The Schrödinger Bridge problem [38, 32] aims to find a stochastic process that connects two arbitrary marginal distributions p_A, p_B while remaining as close as possible to a reference process. When the reference process is a diffusion process initialized at p_A , the solution to the SB problem can be characterized by two coupled partial differential equations (PDEs) governing the forward and backward diffusion processes initialized at p_A and p_B , respectively [23, 48, 4, 5, 26].

SB models are typically trained using iterative proportional fitting which requires expensive simulation of the forward and backward processes [10, 4]. Several approaches have been proposed [33, 39, 47] to improve the scalability of training SB models by leveraging the score and flow matching frameworks [15, 44, 25, 29]. However, SB models overlook the relationships between samples from the two domains, making them unsuitable for paired translation tasks.

Diffusion bridges simplify Schrödinger bridges by assuming a Dirac distribution at one endpoint, allowing them to model the coupling between the two domains for paired translations. I²SB [27] is a diffusion bridge derived from the general theory of SBs. On the other hand, methods like SBALIGN [41], Ω -bridge [30, 31], and DDBM [53] leverage Doob’s h -transform to obtain the formula of a continuous-time h -transformed process that converges almost surely to a specific target sample while aligning closely with the reference diffusion process. SBALIGN and Ω -bridge create a h -transform process that generates data and learn the drift of this process, whereas DDBM designs a h -transformed process that converges to a latent sample. For data generation, DDBM learns the score with respect to the reverse process via conditional score matching, following the approach in [44]. BBDM [24]

extends the unconditional variational framework for discrete-time diffusion processes [13, 19, 42] to a conditional variational framework for Brownian bridges. It then uses the new framework to model the transition kernel of the data generation process.

Different from the aforementioned methods, our method is built on the Chapman-Kolmogorov equation (CKE) for bridges and has a novel design that supports bidirectional transition between the two domains using a single model.

5.2 Diffusion and Flow Models for I2I

Diffusion models (DMs) [40, 43, 13, 44] are powerful generative models that progressively denoise latent samples from a standard Gaussian distribution to generate images. For image-to-image (I2I) translation, DMs can incorporate source images as conditions through either classifier-based [7] or classifier-free [14] guidance techniques during the denoising process to generate corresponding target images [37, 35, 52, 50]. However, since one of the two boundary distributions in DMs is always a standard Gaussian, bidirectional translation requires training two distinct DMs conditioned on source and target images. DDIB [45] exemplifies this approach by combining two separate diffusion models for source and target domains through a shared Gaussian latent space for bidirectional translation.

Flow models (FMs) [29, 25, 1, 8] build an ODE map between two arbitrary boundary distributions and can be trained via the flow matching loss [25] related to the score matching loss for diffusion models [44]. FMs can be viewed as special cases of diffusion bridges where the variance of the transition kernel is zero. Due to their deterministic nature, FMs are less suitable for capturing the coupling between two domains, as demonstrated by our experimental results in Sections 4.2.2 and 4.3.2. Nonetheless, FMs can be useful for unpaired translation and can be specially designed to represent optimal transport maps [28, 25, 46].

6 Conclusion

We introduced the Bidirectional Diffusion Bridge Model (BDBM), a novel framework for bidirectional image-to-image (I2I) translation using a single network. By leveraging the Chapman-Kolmogorov Equation, BDBM models the shared components of forward and backward transitions, enabling efficient bidirectional generation with minimal computational overhead. Empirical results demonstrated that BDBM consistently outperforms existing I2I translation methods across diverse datasets.

Despite these strengths, BDBM has so far been applied exclusively to the image domain. Extending it to other domains, such as text, presents an exciting direction for future research. In particular, exploring BDBM for multimodal tasks like image \leftrightarrow text generation would be a promising avenue.

References

- [1] Michael S Albergo, Nicholas M Boffi, and Eric Vanden-Eijnden. Stochastic interpolants: A unifying framework for flows and diffusions. *arXiv preprint arXiv:2303.08797*, 2023.
- [2] Georgios Batzolis, Jan Stanczuk, Carola-Bibiane Schönlieb, and Christian Etmann. Conditional image generation with score-based diffusion models. *arXiv preprint arXiv:2111.13606*, 2021.
- [3] C Bishop. Pattern recognition and machine learning. *Springer google schola*, 2:531–537, 2006.
- [4] Valentin De Bortoli, James Thornton, Jeremy Heng, and Arnaud Doucet. Diffusion schrödinger bridge with applications to score-based generative modeling. In *NeurIPS*, pages 17695–17709, 2021.
- [5] Tianrong Chen, Guan-Horng Liu, and Evangelos A. Theodorou. Likelihood training of schrödinger bridge using forward-backward sdes theory. In *ICLR*, 2022.
- [6] Jooyoung Choi, Sungwon Kim, Yonghyun Jeong, Youngjune Gwon, and Sungroh Yoon. ILVR: conditioning method for denoising diffusion probabilistic models. In *ICCV*, pages 14347–14356, 2021.
- [7] Prafulla Dhariwal and Alexander Nichol. Diffusion models beat gans on image synthesis. *NeurIPS*, 34:8780–8794, 2021.
- [8] Kien Do, Duc Kieu, Toan Nguyen, Dang Nguyen, Hung Le, Dung Nguyen, and Thin Nguyen. Variational flow models: Flowing in your style. *arXiv preprint arXiv:1312.6114*, 2024.
- [9] Joseph L Doob and JI Doob. *Classical potential theory and its probabilistic counterpart*, volume 262. Springer, 1984.
- [10] Robert Fortet. Résolution d’un système d’équations de m. schrödinger. *Journal de Mathématiques Pures et Appliquées*, 19(1-4):83–105, 1940.
- [11] Ian Goodfellow, Jean Pouget-Abadie, Mehdi Mirza, Bing Xu, David Warde-Farley, Sherjil Ozair, Aaron Courville, and Yoshua Bengio. Generative adversarial nets. *NIPS*, 27:2672–2680, 2014.
- [12] Martin Heusel, Hubert Ramsauer, Thomas Unterthiner, Bernhard Nessler, and Sepp Hochreiter. Gans trained by a two time-scale update rule converge to a local nash equilibrium. *NIPS*, 30:6626–6637, 2017.
- [13] Jonathan Ho, Ajay Jain, and Pieter Abbeel. Denoising diffusion probabilistic models. *NeurIPS*, 33:6840–6851, 2020.
- [14] Jonathan Ho and Tim Salimans. Classifier-free diffusion guidance. In *NeurIPS 2021 Workshop on Deep Generative Models and Downstream Applications*, 2021.
- [15] Aapo Hyvärinen and Peter Dayan. Estimation of non-normalized statistical models by score matching. *Journal of Machine Learning Research*, 6(4), 2005.
- [16] Phillip Isola, Jun-Yan Zhu, Tinghui Zhou, and Alexei A Efros. Image-to-image translation with conditional adversarial networks. *CVPR*, pages 1125–1134, 2017.
- [17] Jack Karush. On the chapman-kolmogorov equation. *The Annals of Mathematical Statistics*, 32(4):1333–1337, 1961.
- [18] Beomsu Kim, Gihyun Kwon, Kwanyoung Kim, and Jong Chul Ye. Unpaired image-to-image translation via neural schrödinger bridge. In *ICLR*, 2024.
- [19] Diederik Kingma, Tim Salimans, Ben Poole, and Jonathan Ho. Variational diffusion models. *NeurIPS*, 34:21696–21707, 2021.
- [20] Diederik P. Kingma and Jimmy Ba. Adam: A method for stochastic optimization. In *ICLR*, 2015.

- [21] Diederik P Kingma and Max Welling. Auto-encoding variational bayes. *ICLR*, 2014.
- [22] Sangyun Lee, Beomsu Kim, and Jong Chul Ye. Minimizing trajectory curvature of ode-based generative models. *ICML*, 202:18957–18973, 2023.
- [23] Christian Léonard. A survey of the schrödinger problem and some of its connections with optimal transport. *Discrete & Continuous Dynamical Systems-A*, 34(4):1533–1574, 2014.
- [24] Bo Li, Kaitao Xue, Bin Liu, and Yu-Kun Lai. BBDM: image-to-image translation with brownian bridge diffusion models. In *CVPR*, pages 1952–1961, 2023.
- [25] Yaron Lipman, Ricky TQ Chen, Heli Ben-Hamu, Maximilian Nickel, and Matthew Le. Flow matching for generative modeling. In *ICLR*, 2022.
- [26] Guan-Horng Liu, Tianrong Chen, Oswin So, and Evangelos A. Theodorou. Deep generalized schrödinger bridge. In *NeurIPS*, 2022.
- [27] Guan-Horng Liu, Arash Vahdat, De-An Huang, Evangelos A. Theodorou, Weili Nie, and Anima Anandkumar. I^2sb : Image-to-image schrödinger bridge. In *ICML*, volume 202, pages 22042–22062, 2023.
- [28] Qiang Liu. Rectified flow: A marginal preserving approach to optimal transport. *arXiv preprint arXiv:2209.14577*, 2022.
- [29] Xingchao Liu, Chengyue Gong, et al. Flow straight and fast: Learning to generate and transfer data with rectified flow. In *ICLR*, 2022.
- [30] Xingchao Liu, Lemeng Wu, Mao Ye, and Qiang Liu. Let us build bridges: Understanding and extending diffusion generative models. In *NeurIPS 2022 Workshop on Score-Based Methods*, 2022.
- [31] Xingchao Liu, Lemeng Wu, Mao Ye, and Qiang Liu. Learning diffusion bridges on constrained domains. In *ICLR*, 2023.
- [32] Michele Pavon and Anton Wakolbinger. On free energy, stochastic control, and schrödinger processes. In *Modeling, Estimation and Control of Systems with Uncertainty: Proceedings of a Conference held in Sopron, Hungary, September 1990*, pages 334–348. Springer, 1991.
- [33] Stefano Peluchetti. Diffusion bridge mixture transports, schrödinger bridge problems and generative modeling. *Journal of Machine Learning Research*, 24(374):1–51, 2023.
- [34] Robin Rombach, Andreas Blattmann, Dominik Lorenz, Patrick Esser, and Björn Ommer. High-resolution image synthesis with latent diffusion models. In *CVPR*, pages 10684–10695, 2022.
- [35] Chitwan Saharia, William Chan, Huiwen Chang, Chris Lee, Jonathan Ho, Tim Salimans, David Fleet, and Mohammad Norouzi. Palette: Image-to-image diffusion models. In *SIGGRAPH*, pages 1–10, 2022.
- [36] Tim Salimans, Ian Goodfellow, Wojciech Zaremba, Vicki Cheung, Alec Radford, and Xi Chen. Improved techniques for training gans. *NeurIPS*, 29:2226–2234, 2016.
- [37] Hiroshi Sasaki, Chris G Willcocks, and Toby P Breckon. Unit-ddpm: Unpaired image translation with denoising diffusion probabilistic models. *arXiv preprint arXiv:2104.05358*, 2021.
- [38] E. Schrödinger. *Über die Umkehrung der Naturgesetze*. Sitzungsberichte der Preussischen Akademie der Wissenschaften. Physikalisch-mathematische Klasse. Verlag der Akademie der Wissenschaften in Kommission bei Walter De Gruyter u. Company, 1931.
- [39] Yuyang Shi, Valentin De Bortoli, Andrew Campbell, and Arnaud Doucet. Diffusion schrödinger bridge matching. In *Proceedings of the 37th International Conference on Neural Information Processing Systems*, pages 62183–62223, 2023.
- [40] Jascha Sohl-Dickstein, Eric Weiss, Niru Maheswaranathan, and Surya Ganguli. Deep unsupervised learning using nonequilibrium thermodynamics. In *ICML*, volume 37, pages 2256–2265, 2015.

- [41] Vignesh Ram Somnath, Matteo Pariset, Ya-Ping Hsieh, María Rodríguez Martínez, Andreas Krause, and Charlotte Bunne. Aligned diffusion schrödinger bridges. In *UAI*, pages 1985–1995, 2023.
- [42] Jiaming Song, Chenlin Meng, and Stefano Ermon. Denoising diffusion implicit models. In *ICLR*, 2021.
- [43] Yang Song and Stefano Ermon. Generative modeling by estimating gradients of the data distribution. *NeurIPS*, pages 11895–11907, 2019.
- [44] Yang Song, Jascha Sohl-Dickstein, Diederik P Kingma, Abhishek Kumar, Stefano Ermon, and Ben Poole. Score-based generative modeling through stochastic differential equations. In *ICLR*, 2021.
- [45] Xuan Su, Jiaming Song, Chenlin Meng, and Stefano Ermon. Dual diffusion implicit bridges for image-to-image translation. In *ICLR*, 2023.
- [46] Alexander Tong, Kilian Fatras, Nikolay Malkin, Guillaume Huguet, Yanlei Zhang, Jarrid Rector-Brooks, Guy Wolf, and Yoshua Bengio. Improving and generalizing flow-based generative models with minibatch optimal transport. *Trans. Mach. Learn. Res.*, 2024.
- [47] Alexander Tong, Nikolay Malkin, Kilian Fatras, Lazar Atanackovic, Yanlei Zhang, Guillaume Huguet, Guy Wolf, and Yoshua Bengio. Simulation-free schrödinger bridges via score and flow matching. *arXiv preprint arXiv:2307.03672*, 2023.
- [48] Francisco Vargas, Pierre Thodoroff, Austen Lamacraft, and Neil Lawrence. Solving schrödinger bridges via maximum likelihood. *Entropy*, 23(9):1134, 2021.
- [49] Igor Vasiljevic, Nick Kolkin, Shanyi Zhang, Ruotian Luo, Haochen Wang, Falcon Z. Dai, Andrea F. Daniele, Mohammadreza Mostajabi, Steven Basart, Matthew R. Walter, and Gregory Shakhnarovich. DIODE: A Dense Indoor and Outdoor DEpth Dataset. *arXiv preprint arXiv:1908.00463*, 2019.
- [50] Julia Wolleb, Robin Sandkühler, Florentin Bieder, and Philippe C Cattin. The swiss army knife for image-to-image translation: Multi-task diffusion models. *arXiv preprint arXiv:2204.02641*, 2022.
- [51] Richard Zhang, Phillip Isola, Alexei A Efros, Eli Shechtman, and Oliver Wang. The unreasonable effectiveness of deep features as a perceptual metric. In *CVPR*, pages 586–595, 2018.
- [52] Min Zhao, Fan Bao, Chongxuan Li, and Jun Zhu. Egsde: Unpaired image-to-image translation via energy-guided stochastic differential equations. *Advances in Neural Information Processing Systems*, 35:3609–3623, 2022.
- [53] Linqi Zhou, Aaron Lou, Samar Khanna, and Stefano Ermon. Denoising diffusion bridge models. In *ICLR*, 2024.

Table of Content for Appendix

| | |
|---|-----------|
| A Theoretical Results | 16 |
| A.1 Derivation of the backward CKE in Eq. 7 from Eq. 6 | 16 |
| A.2 Chapman-Kolmogorov equations for bridges | 16 |
| A.3 Tweedie’s formula for bridges | 17 |
| A.4 Connection between the CKE framework and other frameworks for bridges | 17 |
| A.5 Derivation of transitions in Eq. 17 and Eq. 21 | 20 |
| A.6 Special variants of BDBM | 22 |
| A.7 Training and sampling algorithms for BDBM | 23 |
| B Additional Experimental Results | 23 |
| B.1 Additional qualitative results of BDBM | 23 |
| B.2 Unidirectional translation from color images to sketch/normal maps | 26 |
| B.3 Continuous-time BDBM vs. Discrete-time BDBM | 26 |
| B.4 More visualization on generated samples by BDBM | 27 |

A Theoretical Results

A.1 Derivation of the backward CKE in Eq. 7 from Eq. 6

According to Bayes’ rule, we have:

$$p(x_t|x_T) = \frac{p(x_T|x_t)p(x_t)}{p(x_T)} \quad (25)$$

$$= \frac{p(x_t)}{p(x_T)} \int p(x_T|x_{t+1})p(x_{t+1}|x_t) dx_{t+1} \quad (26)$$

$$= \int \frac{p(x_t)}{p(x_T)} p(x_T|x_{t+1})p(x_{t+1}|x_t) dx_{t+1} \quad (27)$$

$$= \int p(x_{t+1}, x_t) \frac{p(x_T|x_{t+1})}{p(x_T)} dx_{t+1} \quad (28)$$

$$= \int p(x_t|x_{t+1}) \frac{p(x_T|x_{t+1})p(x_{t+1})}{p(x_T)} dx_{t+1} \quad (29)$$

$$= \int p(x_t|x_{t+1})p(x_{t+1}|x_T) dx_{t+1} \quad (30)$$

Here, $p(x_T|x_t) = \int p(x_T|x_{t+1})p(x_{t+1}|x_t) dx_{t+1}$ (from Eq. 25 to Eq. 26) is the backward CKE in Eq. 6. The result in Eq. 30 is the backward CKE in Eq. 7.

A.2 Chapman-Kolmogorov equations for bridges

The CKE for bridges in Eq. 13 can be derived from the CKE for conditional Markov process in Eq. 8 by choosing v to be T . However, deriving the CKE in Eq. 14 from Eq. 8 is not straightforward as it involves the integration w.r.t. dx_t rather than dx_s ($t < s$). It suggests that we should consider the reverse of the original conditional Markov process. Since it is another conditional Markov process

(conditioned on $\hat{x}_0 = y_A$), it can be characterized by the following CKE:

$$p(\hat{x}_T | x_s, \hat{x}_0) = \int p(\hat{x}_T | x_t, \hat{x}_0) p(x_t | x_s, \hat{x}_0) dx_t \quad (31)$$

$$\Rightarrow \frac{p(x_s | \hat{x}_T, \hat{x}_0) p(\hat{x}_T | \hat{x}_0)}{p(x_s | \hat{x}_0)} = \int \frac{p(x_t | \hat{x}_T, \hat{x}_0) p(\hat{x}_T | \hat{x}_0)}{p(x_t | \hat{x}_0)} p(x_t | x_s, \hat{x}_0) dx_t \quad (32)$$

$$\Rightarrow p(x_s | \hat{x}_T, \hat{x}_0) = \int \frac{p(x_t | x_s, \hat{x}_0) p(x_s | \hat{x}_0)}{p(x_t | \hat{x}_0)} p(x_t | \hat{x}_T, \hat{x}_0) dx_t \quad (33)$$

$$\Rightarrow p(x_s | \hat{x}_T, \hat{x}_0) = \int p(x_s | x_t, \hat{x}_0) p(x_t | \hat{x}_T, \hat{x}_0) dx_t \quad (34)$$

Here, $\hat{x}_T \sim p(\hat{x}_T | \hat{x}_0)$ with $p(\hat{x}_T = y_B) = p(y_B | y_A)$. By writing Eq. 33 with slightly different notations, we obtain Eq. 14.

A.3 Tweedie's formula for bridges

Assume that x is sampled from a Gaussian distribution $p(x | y_A, y_B) = \mathcal{N}(\alpha y_A + \beta y_B, \sigma^2 \mathbf{I})$. The posterior expectation of y_B given x and y_A can be computed as follows:

$$\tilde{y}_B = \mathbb{E}_{p(y_B | x, y_A)}[y_B] = x - \alpha y_A + \sigma^2 \nabla \log p(x | y_A) \quad (35)$$

where $p(x | y_A) = \mathbb{E}_{p(y_B | y_A)}[p(x | y_A, y_B)]$. We refer to Eq. 35 as Tweedie's formula for bridges.

We start by representing $\nabla \log p(x | y_A)$ as follows:

$$\nabla \log p(x | y_A) \quad (36)$$

$$= \frac{1}{p(x | y_A)} \nabla p(x | y_A) \quad (37)$$

$$= \frac{1}{p(x | y_A)} \nabla \int p(x | y_A, y_B) p(y_B | y_A) dy_B \quad (38)$$

$$= \frac{1}{p(x | y_A)} \int p(y_B | y_A) \nabla p(x | y_A, y_B) dy_B \quad (39)$$

$$= \int \frac{p(y_B | y_A) p(x | y_A, y_B)}{p(x | y_A)} \nabla \log p(x | y_A, y_B) dy_B \quad (40)$$

$$= \int p(y_B | x, y_A) \left(\frac{\alpha y_A + \beta y_B - x}{\sigma^2} \right) dy_B \quad (41)$$

$$= \frac{\alpha y_A + \beta \mathbb{E}_{p(y_B | x, y_A)}[y_B] - x}{\sigma^2} \quad (42)$$

Rearrange Eq. 42, we have:

$$\tilde{y}_B = \mathbb{E}_{p(y_B | x, y_A)}[y_B] = \frac{1}{\beta} (x - \alpha y_A + \sigma^2 \nabla \log p(x | y_A)) \quad (43)$$

Since $p(x | y_A, y_B) = \mathcal{N}(\alpha y_A + \beta y_B, \sigma^2 \mathbf{I})$, x can be represented as $x = \alpha y_A + \beta y_B + \sigma z$, which means:

$$y_B = \frac{1}{\beta} (x - \alpha y_A - \sigma z) \quad (44)$$

Eqs. 43, 44 suggest that $-\sigma \nabla \log p(x | y_A)$ is the least square approximation of z . This means $z_\theta(t, x_t, x_0)$ in Eq. 19 should equal to $-\sigma \nabla \log p(x | x_0)$.

A.4 Connection between the CKE framework and other frameworks for bridges

A.4.1 Link to variational inference

If we assume the generative process is a discrete-time *conditional Markov process* running from time 0 to time T with the initial distribution $p(x_0 | \hat{x}_0)$ being a Dirac distribution at \hat{x}_0 (i.e., $p(x_0 | \hat{x}_0) = \delta_{\hat{x}_0}$), the generative distribution over all time steps will be given below:

$$p_\theta(x_{0:T} | \hat{x}_0) = p(x_0 | \hat{x}_0) \prod_{t=0}^{T-1} p_\theta(x_{t+1} | x_t, \hat{x}_0) \quad (45)$$

Here, x_0, \dots, x_{T-1} are regarded as latent variables and x_T is regarded as an observed variable. The (variational) inference distribution $q(x_{0:T-1}|\hat{x}_T, \hat{x}_0)$ can be factorized as follows:

$$\begin{aligned} & q(x_{0:T-1}|\hat{x}_T, \hat{x}_0) \\ &= q(x_{T-1}|\hat{x}_T, \hat{x}_0) \prod_{t=0}^{T-2} q(x_t|x_{t+1}, \hat{x}_T, \hat{x}_0) \end{aligned} \quad (46)$$

$$= q(x_{T-1}|\hat{x}_T, \hat{x}_0) \prod_{t=0}^{T-2} \frac{q(x_{t+1}|x_t, \hat{x}_T, \hat{x}_0) q(x_t|\hat{x}_T, \hat{x}_0)}{q(x_{t+1}|\hat{x}_T, \hat{x}_0)} \quad (47)$$

$$= q(x_0|\hat{x}_T, \hat{x}_0) \prod_{t=0}^{T-2} q(x_{t+1}|x_t, \hat{x}_T, \hat{x}_0) \quad (48)$$

which characterizes a double conditional Markov process with Dirac distributions $\delta_{\hat{x}_0}$ and $\delta_{\hat{x}_T}$ at both ends and the transition kernel $q(x_{t+1}|x_t, \hat{x}_T, \hat{x}_0)$.

We can learn θ by minimizing the negative variational lower bound below:

$$\begin{aligned} & -\mathbb{E}_{p(\hat{x}_0)p(\hat{x}_T|\hat{x}_0)} [\text{ELBO}(\hat{x}_T, \hat{x}_0)] \\ &= \mathbb{E}_{p(\hat{x}_0)p(\hat{x}_T|\hat{x}_0)} \left[\mathbb{E}_{q(x_{0:T-1}|\hat{x}_T, \hat{x}_0)} \left[-\log \frac{p_\theta(x_{0:T}|\hat{x}_0)}{q(x_{0:T-1}|\hat{x}_T, \hat{x}_0)} \right] \right] \quad (49) \\ &= -\log p_\theta(x_T|x_{T-1}, \hat{x}_0) \\ & \quad + \sum_{t=1}^{T-1} D_{\text{KL}}(q(x_{t+1}|x_t, \hat{x}_T, \hat{x}_0) \| p_\theta(x_{t+1}|x_t, \hat{x}_0)) \\ & \quad + D_{\text{KL}}(q(x_0|\hat{x}_T, \hat{x}_0) \| p(x_0|\hat{x}_0)) \end{aligned} \quad (50)$$

The KL term in Eq. 50 is the discrete-time version of our loss in Eq. 15.

A.4.2 Link to score matching

When the Markov process between \hat{x}_0, \hat{x}_T is a continuous-time diffusion process, the problem of matching $p_\theta(x_s|x_t, \hat{x}_0)$ to $q(x_s|x_t, \hat{x}_T, \hat{x}_0)$ in Eq. 15 can be reformulated in the differential form as matching $\frac{\partial}{\partial t} p_\theta(x_t|\hat{x}_0)$ to $\frac{\partial}{\partial t} q(x_t|\hat{x}_T, \hat{x}_0)$ where $q(x_t|\hat{x}_T, \hat{x}_0)$ is the marginal distribution at time t of the diffusion process between \hat{x}_0, \hat{x}_T . Given the connection between $\frac{\partial p}{\partial t}$ and ∇p via the KBE (Eq. 3), we can instead match $\nabla p_\theta(x_t|\hat{x}_0)$ to $\nabla q(x_t|\hat{x}_T, \hat{x}_0)$, which is similar to matching $\nabla \log p_\theta(x_t|\hat{x}_0)$ to $\nabla \log q(x_t|\hat{x}_T, \hat{x}_0)$.

A.4.3 Link to Doob's h -transform

We consider a slightly different setting for bridges: Instead of starting a Markov process from a specific initial sample $\hat{x}_0 = y_A$ and ensure that the final distribution $p(x_T|\hat{x}_0)$ will satisfy $p(x_T = y_B|\hat{x}_0) = p(y_B|y_A)$, we start the process from an initial distribution of x_0 and force it to hit a predetermined sample $\hat{x}_T = y_B$ at time T almost surely. If the initial distribution $p(x_0)$ is chosen such that $p(x_0 = y_A) = p(y_A|y_B)$, then the two settings are statistically equivalent when all samples from the two domains A, B are counted.

Let $p(x_t)$ be the marginal distribution at time t corresponding to a Markov process starting from the initial distribution $p(x_0)$. Also assume that $p(x_t)$ has support over the entire sample space. Then, we have:

$$p(\hat{x}_T) = \int p(\hat{x}_T|x_t) p(x_t) dx_t \quad (51)$$

Interestingly, we can define a *new* marginal distribution of x_t as $\tilde{p}(x_t) = \frac{p(\hat{x}_T|x_t)p(x_t)}{p(\hat{x}_T)}$, and if this distribution converges to a Dirac distribution at time T then, under some mild conditions², this Dirac distribution should center around $\hat{x}_T = y_B$.

²A key condition here is that $\hat{p}(x_t = y_B)$ does not vanish $\forall t$.

At time $s \neq t$, Eq. 51 becomes:

$$p(\hat{x}_T) = \int p(\hat{x}_T|x_s) p(x_s) dx_s \quad (52)$$

$$= \int p(\hat{x}_T|x_s) \left(\int p(x_s|x_t) p(x_t) dx_t \right) dx_s \quad (53)$$

$$= \int \int p(\hat{x}_T|x_s) p(x_s|x_t) p(x_t) dx_t dx_s \quad (54)$$

$$= \int \left(\int p(\hat{x}_T|x_s) p(x_s|x_t) dx_s \right) p(x_t) dx_t \quad (55)$$

Since $p(\hat{x}_T)$ in Eq. 51 is the same as in Eq. 55, the CKE below should hold for every $s \neq t$:

$$p(\hat{x}_T|x_t) = \int p(\hat{x}_T|x_s) p(x_s|x_t) dx_s \quad (56)$$

$$= \mathbb{E}[p(\hat{x}_T|X_s) | X_t = x_t] \quad (57)$$

Here, we focus on the generative setting with $0 < t < s$ and rewrite Eq. 56 as follows:

$$1 = \int p(x_s|x_t) \frac{p(\hat{x}_T|x_s)}{p(\hat{x}_T|x_t)} dx_s \quad (58)$$

Eq. 58 suggests that we can set $p(x_s|x_t) \frac{p(\hat{x}_T|x_s)}{p(\hat{x}_T|x_t)}$ to be a distribution over x_s . Let us denote $\tilde{p}(x_s|x_t) = p(x_s|x_t) \frac{p(\hat{x}_T|x_s)}{p(\hat{x}_T|x_t)}$, then $\tilde{p}(x_s|x_t)$ can be viewed as the transition kernel of another Markov process derived from the original Markov process. Interestingly, $\tilde{p}(x_t)$ is the marginal distribution at time t of this process, and since $\tilde{p}(\hat{x}_T)$ is a Dirac distribution at \hat{x}_T , this process converges to $\hat{x}_T = y_B$ almost surely. Please refer to the last part of this subsection for detail proofs.

It is worth noting that in Eq. 51, the term $p(x_t)$ is fixed since it is the marginal distribution of the (predefined) original Markov process while the term $p(\hat{x}_T|x_t)$ can vary freely as long as it satisfies Eq. 56. Therefore, if we let $h(\cdot, \cdot, T, \hat{x}_T)$ be any function such that:

$$h(t, x_t, T, \hat{x}_T) = \int h(s, x_s, T, \hat{x}_T) p(x_s|x_t) dx_s \quad (59)$$

$$= \mathbb{E}[h(s, X_s, T, \hat{x}_T) | X_t = x_t] \quad (60)$$

and $h(T, x_T, T, \hat{x}_T) = \delta_{\hat{x}_T}(x_T)$ then by setting $\tilde{p}(x_s|x_t) = p(x_s|x_t) \frac{h(s, x_s, T, \hat{x}_T)}{h(t, x_t, T, \hat{x}_T)}$, we obtain a new Markov process called *Doob's h-transform process* that converges to $\hat{x}_T = y_B$ almost surely. This is the main idea behind Doob's *h-transform* [9].

In the continuous-time setting, Eq. 56 can be written in the differential form below:

$$\begin{cases} \mathcal{A}_t h(t, x_t, T, \hat{x}_T) = 0 \\ h(T, x_T, T, \hat{x}_T) = \delta_{\hat{x}_T}(x_T) \end{cases} \quad (61)$$

where \mathcal{A}_t is the generator operator defined as $\mathcal{A}_t f(t, x_t) \triangleq \lim_{\Delta t \downarrow 0} \frac{\mathbb{E}[f(t+\Delta t, X_{t+\Delta t}) | X_t = x_t] - f(t, x_t)}{\Delta t}$. The above equation is in fact a KBE. When the original Markov process is a continuous-time diffusion process described by the SDE $dX_t = \mu(t, X_t) dt + \sigma(t) dW_t$, given any real-valued function $f(t, x)$, $\mathcal{A}_t f(t, x)$ can be represented as follows:

$$\begin{aligned} \mathcal{A}_t f &= \frac{\partial f}{\partial t} + \nabla f \cdot \mu + \frac{\sigma^2}{2} \Delta f \\ &= \frac{\partial f}{\partial t} + \mathcal{G}f \end{aligned}$$

The generator \mathcal{A}_t^h of the *Doob's h-transform process* can be derived from \mathcal{A}_t as follows:

$$\mathcal{A}_t^h f = \frac{1}{h} \mathcal{A}_t (fh)$$

By leveraging the fact that $\mathcal{A}_t h = 0$ in Eq. 61, $\mathcal{A}_t^h f$ can be expressed as follows:

$$\mathcal{A}_t^h f = \frac{\partial f}{\partial t} + \nabla f \cdot (\mu + \sigma^2 \nabla \log h) + \frac{\sigma^2}{2} \Delta f$$

It implies that this diffusion process is described by the SDE:

$$dX_t = (\mu(t, X_t) + \sigma^2 \nabla \log h(t, X_t, T, \hat{x}_T)) dt + \sigma(t) dW_t$$

Proofs for some properties of $\tilde{p}(x_s|x_t)$ and $\tilde{p}(x_t)$ For any times $0 \leq t < r < s$, we have:

$$\begin{aligned} & \int \tilde{p}(x_s|x_r) \tilde{p}(x_r|x_t) dx_r \\ &= \int p(x_s|x_r) \frac{p(\hat{x}_T|x_s)}{p(\hat{x}_T|x_r)} p(x_r|x_t) \frac{p(\hat{x}_T|x_r)}{p(\hat{x}_T|x_t)} dx_r \end{aligned} \quad (62)$$

$$= \frac{p(\hat{x}_T|x_s)}{p(\hat{x}_T|x_t)} \int p(x_s|x_r) p(x_r|x_t) dx_r \quad (63)$$

$$= \frac{p(\hat{x}_T|x_s)}{p(\hat{x}_T|x_t)} p(x_s|x_t) \quad (64)$$

$$= \tilde{p}(x_s|x_t) \quad (65)$$

The last equation implies that $\tilde{p}(x_s|x_t)$ satisfies the CKE and is the transition probability of a Markov process. Besides, we have:

$$\begin{aligned} & \int \tilde{p}(x_s|x_t) \tilde{p}(x_t) dx_t \\ &= \int p(x_s|x_t) \frac{p(\hat{x}_T|x_s)}{p(\hat{x}_T|x_t)} \frac{p(\hat{x}_T|x_t)}{p(\hat{x}_T)} p(x_t) dx_t \end{aligned} \quad (66)$$

$$= \frac{p(\hat{x}_T|x_s)}{p(\hat{x}_T)} \int p(x_s|x_t) p(x_t) dx_t \quad (67)$$

$$= \frac{p(\hat{x}_T|x_s) p(x_s)}{p(\hat{x}_T)} \quad (68)$$

$$= \tilde{p}(x_s) \quad (69)$$

which means $\tilde{p}(x_t)$ is the marginal distribution at time t of the Markov process characterized by $\tilde{p}(x_s|x_t)$.

A.5 Derivation of transitions in Eq. 17 and Eq. 21

We consider the case where marginal distributions at timestep t and s (with $t < s$) are $q(x_t|x_0, x_T) = \mathcal{N}(\alpha_t x_0 + \beta_t x_T, \sigma_t^2 \mathbf{I})$ and $q(x_s|x_0, x_T) = \mathcal{N}(\alpha_s x_0 + \beta_s x_T, \sigma_s^2 \mathbf{I})$, respectively. We detail the derivation of our proposed forward transition distribution, denoted as $q(x_s|x_t, x_0, x_T)$, and backward transition distribution, denoted as $q(x_t|x_s, x_0, x_T)$.

A.5.1 Derivation of forward transition $q(x_s|x_t, x_0, x_T)$ in Eq. 17

Recall that the forward CKE, from t to s , given two endpoints x_0 and x_T is given by:

$$q(x_s|x_0, x_T) = \int q(x_s|x_t, x_0, x_T) q(x_t|x_0, x_T) dx_t$$

where $q(x_s|x_t, x_0, x_T)$ replace $p_\theta(x_s|x_t, x_0)$ in Eq. 14 in case we align $p_\theta(x_s|x_t, \hat{x}_0)$ with $q(x_s|x_t, \hat{x}_T, \hat{x}_0)$. Following [3] (Eq. 2.115), we assume that $q(x_s|x_t, x_0, x_T) = \mathcal{N}(ax_t + bx_0 + cx_T + d, \delta_{s,t}^2 \mathbf{I})$ and we have:

$$\mathbb{E} \begin{bmatrix} x_t|x_0, x_T \\ x_s|x_t, x_0, x_T \end{bmatrix} = \begin{pmatrix} \alpha_t x_0 + \beta_t x_T \\ a(\alpha_t x_0 + \beta_t x_T) + bx_0 + cx_T + d \end{pmatrix} \quad (70)$$

$$\text{Cov} = \begin{pmatrix} \text{diag}(\sigma_t^2) & \text{diag}(a\sigma_t^2) \\ \text{diag}(a\sigma_t^2) & \text{diag}(\delta_{s,t}^2 + a^2\sigma_t^2) \end{pmatrix} \quad (71)$$

Compare the mean and covariance with that of $q(x_s | x_0, x_T)$, we have:

$$\begin{cases} d = 0 \\ a(\alpha_t x_0 + \beta_t x_T) + b x_0 + c x_T = \alpha_s x_0 + \beta_s x_T \\ \delta_{s,t}^2 + a^2 \sigma_t^2 = \sigma_s^2 \end{cases} \quad (72)$$

$$\Rightarrow \begin{cases} a = \frac{\sqrt{\sigma_s^2 - \delta_{s,t}^2}}{\sigma_t} \\ b = \alpha_s - \alpha_t \frac{\sqrt{\sigma_s^2 - \delta_{s,t}^2}}{\sigma_t} \\ c = \beta_s - \beta_t \frac{\sqrt{\sigma_s^2 - \delta_{s,t}^2}}{\sigma_t} \end{cases} \quad (73)$$

$$\begin{aligned} & q(x_s | x_t, x_0, x_T) \\ &= \mathcal{N} \left(\left(\frac{\sqrt{\sigma_s^2 - \delta_{s,t}^2}}{\sigma_t} \right) x_t + \left(\alpha_s - \alpha_t \frac{\sqrt{\sigma_s^2 - \delta_{s,t}^2}}{\sigma_t} \right) x_0 + \left(\beta_s - \beta_t \frac{\sqrt{\sigma_s^2 - \delta_{s,t}^2}}{\sigma_t} \right) x_T, \delta_{s,t}^2 \mathbf{I} \right) \end{aligned} \quad (74)$$

$$= \mathcal{N} \left(\alpha_s x_0 + \beta_s x_T + \sqrt{\sigma_s^2 - \delta_{s,t}^2} \frac{(x_t - \alpha_t x_0 - \beta_t x_T)}{\sigma_t}, \delta_{s,t}^2 \mathbf{I} \right) \quad (75)$$

A.5.2 Derivation of backward transition $q(x_t | x_s, x_0, x_T)$ in Eq. 21

Recall that from 20, we can derive $q(x_t | x_s, x_0, x_T)$ from Bayes' rule:

$$q(x_t | x_s, x_0, x_T) = q(x_s | x_t, x_0, x_T) \frac{q(x_t | x_0, x_T)}{q(x_s | x_0, x_T)} \quad (76)$$

With:

$$\begin{aligned} & q(x_s | x_t, x_0, x_T) \\ &= \frac{1}{\sqrt{2\pi} \delta_{s,t}} \exp \left(-\frac{1}{2} \frac{\left(x_s - \left(\frac{\sqrt{\sigma_s^2 - \delta_{s,t}^2}}{\sigma_t} x_t + \left(\alpha_s - \alpha_t \frac{\sqrt{\sigma_s^2 - \delta_{s,t}^2}}{\sigma_t} \right) x_0 + \left(\beta_s - \beta_t \frac{\sqrt{\sigma_s^2 - \delta_{s,t}^2}}{\sigma_t} \right) x_T \right) \right)^2}{\delta_{s,t}^2} \right) \end{aligned} \quad (77)$$

$$q(x_t | x_0, x_T) = \frac{1}{\sqrt{2\pi} \sigma_t} \exp \left(-\frac{1}{2} \frac{(x_t - (\alpha_t x_0 + \beta_t x_T))^2}{\sigma_t^2} \right) \quad (78)$$

$$q(x_s | x_0, x_T) = \frac{1}{\sqrt{2\pi} \sigma_s} \exp \left(-\frac{1}{2} \frac{(x_s - (\alpha_s x_0 + \beta_s x_T))^2}{\sigma_s^2} \right) \quad (79)$$

Then we know:

$$\begin{aligned} & q(x_t | x_s, x_0, x_T) \\ &= \frac{1}{\sqrt{2\pi} \frac{\delta_{s,t} \sigma_t}{\sigma_s}} \exp \left[-\frac{1}{2} \left(\frac{\left(x_s - \left(\frac{\sqrt{\sigma_s^2 - \delta_{s,t}^2}}{\sigma_t} x_t + \left(\alpha_s - \alpha_t \frac{\sqrt{\sigma_s^2 - \delta_{s,t}^2}}{\sigma_t} \right) x_0 + \left(\beta_s - \beta_t \frac{\sqrt{\sigma_s^2 - \delta_{s,t}^2}}{\sigma_t} \right) x_T \right) \right)^2}{\delta_{s,t}^2} \right. \right. \\ & \left. \left. + \frac{(x_t - (\alpha_t x_0 + \beta_t x_T))^2}{\sigma_t^2} - \frac{(x_s - (\alpha_s x_0 + \beta_s x_T))^2}{\sigma_s^2} \right) \right] \end{aligned} \quad (80)$$

$$= \frac{1}{\sqrt{2\pi} \frac{\delta_{s,t} \sigma_t}{\sigma_s}} \exp \left(-\frac{(x_t - \tilde{\mu}_t)^2}{2 \left(\frac{\delta_{s,t} \sigma_t}{\sigma_s} \right)^2} \right) \quad (81)$$

where

$$\begin{aligned}\tilde{\mu}_t &= \left(\frac{\sigma_t \sqrt{\sigma_s^2 - \delta_{s,t}^2}}{\sigma_s^2} \right) x_s + \left(\alpha_t - \alpha_s \frac{\sigma_t \sqrt{\sigma_s^2 - \delta_{s,t}^2}}{\sigma_s^2} \right) x_0 + \left(\beta_t - \beta_s \frac{\sigma_t \sqrt{\sigma_s^2 - \delta_{s,t}^2}}{\sigma_s^2} \right) x_T \\ &= \alpha_t x_0 + \beta_t x_T + \sigma_t \sqrt{\sigma_s^2 - \delta_{s,t}^2} \frac{(x_s - \alpha_s x_0 - \beta_s x_T)}{\sigma_s^2}\end{aligned}\quad (82)$$

A.6 Special variants of BDBM

Below, we discuss several important variants of BDBM. These variants mainly correspond to the variability of $\delta_{s,t}$ within the interval $[0, \sigma_s)$.

A.6.1 $\delta_{s,t} = 0$

If we set $\delta_{s,t} = 0$, then $p_\theta(x_s|x_t, x_0)$ will become the deterministic mapping $\mu_\theta(s, t, x_t, x_0)$ from x_t, x_0 to x_s . Similarly, $p_\phi(x_t|x_s, x_T)$ will become the deterministic mapping $\tilde{\mu}_\phi(t, s, x_s, x_T)$ from x_s, x_T to x_t . This variant links to the deterministic mapping from $x_t(x)$ to $x(x_t)$ in DDIM [42].

A.6.2 $\delta_{s,t} = \sqrt{\sigma_s^2 - \sigma_t^2 \frac{\beta_s^2}{\beta_t^2}}$

When $\delta_{s,t} = \sqrt{\sigma_s^2 - \sigma_t^2 \frac{\beta_s^2}{\beta_t^2}}$, $\mu(s, t, x_t, x_0, x_T)$ (Eq. 17) and $\tilde{\mu}(t, s, x_s, x_0, x_T)$ (Eq. 21) become:

$$\mu(s, t, x_t, x_0, x_T) = \frac{\beta_s}{\beta_t} x_t + \left(\alpha_s - \alpha_t \frac{\beta_s}{\beta_t} \right) x_0 \quad (83)$$

$$\tilde{\mu}(t, s, x_s, x_0, x_T) = \frac{\sigma_t^2 \beta_s}{\sigma_s^2 \beta_t} x_s + \left(\alpha_t - \alpha_s \frac{\sigma_t^2 \beta_s}{\sigma_s^2 \beta_t} \right) x_0 + \left(\beta_t - \beta_s \frac{\sigma_t^2 \beta_s}{\sigma_s^2 \beta_t} \right) x_T \quad (84)$$

Although the term containing x_T in Eq. 83 vanishes, $\mu(s, t, x_t, x_0, x_T)$ still depends on x_T since x_t depends on x_T via Eq. 16. In this case, if x_T is modeled directly via $x_{T,\theta}$, then setting $x_t = x_0$ at the initial sampling step $t = 0$ will lead to poor generation results since $\mu_\theta(t, x_t, x_0)$ no longer depends on $x_{T,\theta}(t, x_t, x_0)$. Instead, we have to set $x_t = \alpha_\epsilon x_0 + \beta_\epsilon x_{T,\theta}(\epsilon, x_0, x_0)$ where ϵ is a small value such that $\beta_\epsilon \neq \beta_0 = 0$. This will ensure that $\mu_\theta(t, x_t, x_0)$ uses the knowledge from $x_{T,\theta}(\epsilon, x_0, x_0)$.

The term containing x_T in Eq. 84 is unlikely to vanish because otherwise, this will lead to $\frac{\beta_t}{\beta_s} = \frac{\sigma_t}{\sigma_s}$ for every time pair (t, s) . This equation does not hold since if we choose $t = T$ and choose s such that $\beta_s, \sigma_s \neq 0$, we have $\frac{\beta_T}{\beta_s} = \frac{1}{\beta_s} \neq \frac{0}{\sigma_s} = \frac{\sigma_T}{\sigma_s}$. The term containing x_0 in Eq. 84, by contrast, can vanish if $\alpha_t - \alpha_s \frac{\sigma_t^2 \beta_s}{\sigma_s^2 \beta_t} = 0$, or equivalently, $\sigma_t^2 = k \alpha_t \beta_t$ where $k > 0$ is a constant w.r.t. t .

A.6.3 $\delta_{s,t} = \sqrt{\sigma_s^2 - \sigma_t^2 \frac{\alpha_s^2}{\alpha_t^2}}$

When $\delta_{s,t} = \sqrt{\sigma_s^2 - \sigma_t^2 \frac{\alpha_s^2}{\alpha_t^2}}$, $\mu(s, t, x_t, x_0, x_T)$ and $\tilde{\mu}(t, s, x_s, x_0, x_T)$ become:

$$\mu(s, t, x_t, x_0, x_T) = \frac{\alpha_s}{\alpha_t} x_t + \left(\beta_s - \beta_t \frac{\alpha_s}{\alpha_t} \right) x_T \quad (85)$$

$$\tilde{\mu}(t, s, x_s, x_0, x_T) = \frac{\sigma_t^2 \alpha_s}{\sigma_s^2 \alpha_t} x_s + \left(\alpha_t - \alpha_s \frac{\sigma_t^2 \alpha_s}{\sigma_s^2 \alpha_t} \right) x_0 + \left(\beta_t - \beta_s \frac{\sigma_t^2 \alpha_s}{\sigma_s^2 \alpha_t} \right) x_T \quad (86)$$

In this case, there will be no problem during sampling with $\mu_\theta(t, x_t, x_0)$ and $\mu_\phi(s, x_s, x_T)$ since they always use the knowledge from $x_{T,\theta}(t, x_t, x_0)$ and $x_{0,\phi}(s, x_s, x_T)$, respectively. Note that the term containing x_T in Eq. 86 can vanish if $\sigma_t^2 = k \alpha_t \beta_t$ ($k > 0$) but this does not affect sampling.

A.6.4 Brownian Bridge

A Brownian Bridge [24] is a special case of the generalized diffusion bridge in which:

$$\begin{aligned}\beta_t &= \frac{t}{T} \\ \alpha_t &= 1 - \beta_t = 1 - \frac{t}{T} \\ \sigma_t^2 &= k\alpha_t\beta_t = k\frac{t}{T}\left(1 - \frac{t}{T}\right)\end{aligned}$$

With this choice of α_t , β_t , and σ_t , we can easily prove that $\sigma_s^2 - \sigma_t^2 \frac{\alpha_s^2}{\alpha_t^2} \geq 0$ for all $t < s$ as follows:

$$\begin{aligned}\sigma_s^2 - \sigma_t^2 \frac{\alpha_s^2}{\alpha_t^2} &\geq 0 \\ \Leftrightarrow \frac{\sigma_s^2}{\sigma_t^2} &\geq \frac{\alpha_s^2}{\alpha_t^2} \\ \Leftrightarrow \frac{\beta_s}{\beta_t} &\geq \frac{\alpha_s}{\alpha_t} \\ \Leftrightarrow \frac{s}{t} &\geq \frac{T-s}{T-t} \\ \Leftrightarrow sT &\geq tT \\ \Leftrightarrow s &\geq t\end{aligned}$$

Therefore, we can set $\delta_{s,t} = \sqrt{\eta \left(\sigma_s^2 - \sigma_t^2 \frac{\alpha_s^2}{\alpha_t^2} \right)}$ with $\eta \in [0, 1]$.

When $\eta = 1$, $\mu(s, t, x_t, x_0, x_T)$ and $\tilde{\mu}(t, s, x_s, x_0, x_T)$ become:

$$\mu(s, t, x_t, x_0, x_T) = \frac{\alpha_s}{\alpha_t} x_t + \left(\beta_s - \beta_t \frac{\alpha_s}{\alpha_t} \right) x_T \quad (87)$$

$$= \frac{T-s}{T-t} x_t + \frac{(s-t)T}{T-t} x_T \quad (88)$$

$$\tilde{\mu}(t, s, x_s, x_0, x_T) = \frac{\sigma_t^2}{\sigma_s^2} \frac{\alpha_s}{\alpha_t} x_s + \left(\alpha_t - \alpha_s \frac{\sigma_t^2}{\sigma_s^2} \frac{\alpha_s}{\alpha_t} \right) x_0 \quad (89)$$

$$= \frac{\beta_t}{\beta_s} x_s + \left(\alpha_t - \alpha_s \frac{\beta_t}{\beta_s} \right) x_0 \quad (90)$$

$$= \frac{t}{s} x_s + \frac{(s-t)T}{s} x_0 \quad (91)$$

A.7 Training and sampling algorithms for BDBM

In Algos. 1,2, and 3, we provide the detailed training, forward sampling and backward sampling algorithms for our proposed BDBM with $z_\varphi(t, x_t, (1-m) * x_0, m * x_T)$ as the model.

B Additional Experimental Results

B.1 Additional qualitative results of BDBM

Figs. 6, 7, and 8 showcase BDBM's generated samples for both translation directions on the Edges \leftrightarrow Shoes, Edges \leftrightarrow Handbag, and Night \leftrightarrow Day datasets. Input samples are taken from a held-out test set not used during training. The results demonstrate high-quality and diverse outputs, highlighting BDBM's effectiveness in bidirectional translation.

Algorithm 1 Training BDBM

- 1: **Input:** $\alpha_t, \beta_t, \sigma_t$ as continuously differentiable functions of t satisfying $\alpha_0 = \beta_T = 1$ and $\alpha_T = \beta_0 = \sigma_0 = \sigma_T = 0$
 - 2: **repeat**
 - 3: $t \sim \mathcal{U}(0, T)$
 - 4: $x_0, x_T \sim p(y_A, y_B)$
 - 5: $z \sim \mathcal{N}(0, \mathbf{I})$
 - 6: $x_t = \alpha_t x_0 + \beta_t x_T + \sigma_t z$
 - 7: $m \sim \mathcal{B}(0.5)$
 - 8: Update φ by minimizing $\mathcal{L}(\varphi) = \|z_\varphi(t, x_t, (1-m) * x_0, m * x_T) - z\|_2^2$
 - 9: **until** converged
-

Algorithm 2 Generating x_T given x_0 (forward)

- 1: **Input:** $\alpha_t, \beta_t, \sigma_t, \delta_{s,t}$, trained $z_\varphi(t, x_t, (1-m) * x_0, m * x_T), x_0$
 - 2: $m = 0$
 - 3: **for** $t = 0$ **to** $T - \Delta t$ **do**
 - 4: $s = t + \Delta t$
 - 5: $z_{t|0} = z_\varphi(t, x_t, x_0, 0)$
 - 6: **if** $s = T$ **then**
 - 7: $\epsilon = 0$
 - 8: **else**
 - 9: $\epsilon \sim \mathcal{N}(0, \mathbf{I})$
 - 10: **end if**
 - 11: $x_s = \frac{\beta_s}{\beta_t} x_t + \left(\alpha_s - \alpha_t \frac{\beta_s}{\beta_t}\right) x_0 + \left(\sqrt{\sigma_s^2 - \delta_{s,t}^2} - \sigma_t \frac{\beta_s}{\beta_t}\right) z_{t|0} + \delta_{s,t} \epsilon$
 - 12: **end for**
 - 13: **return** x_s
-

Algorithm 3 Generating x_0 given x_T (backward)

- 1: **Input:** $\alpha_t, \beta_t, \sigma_t, \delta_{s,t}$, trained $z_\varphi(t, x_t, (1-m) * x_0, m * x_T), x_T$
 - 2: $m = 1$
 - 3: **for** $s = T$ **to** Δt **do**
 - 4: $t = s - \Delta t$
 - 5: $z_{s|T} = z_\varphi(s, x_s, 0, x_T)$
 - 6: **if** $t = 0$ **then**
 - 7: $\epsilon = 0$
 - 8: **else**
 - 9: $\epsilon \sim \mathcal{N}(0, \mathbf{I})$
 - 10: **end if**
 - 11: $x_t = \frac{\alpha_t}{\alpha_s} x_s + \left(\beta_t - \beta_s \frac{\alpha_t}{\alpha_s}\right) x_T + \left(\frac{\sigma_t \sqrt{\sigma_s^2 - \delta_{s,t}^2}}{\sigma_s} - \sigma_s \frac{\alpha_t}{\alpha_s}\right) z_{s|T} + \frac{\delta_{s,t} \sigma_t}{\sigma_s} \epsilon$
 - 12: **end for**
 - 13: **return** x_t
-

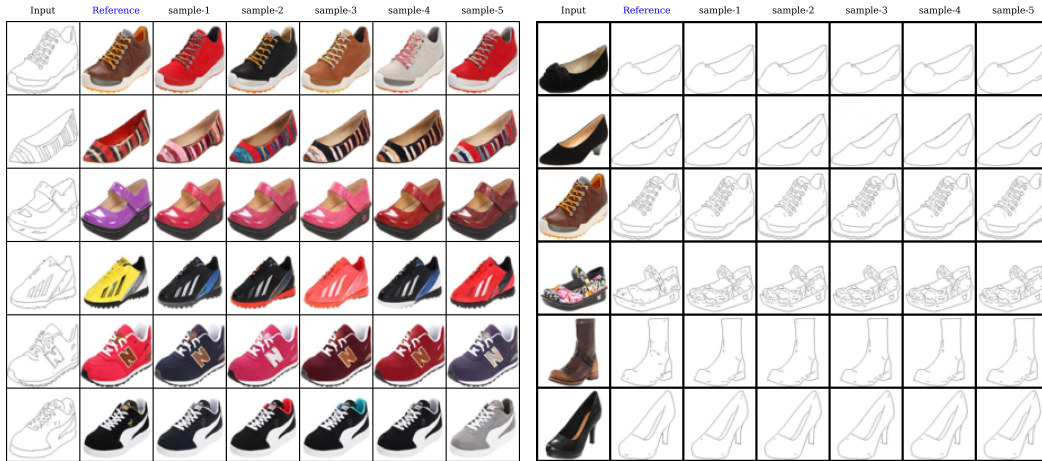


Figure 6: Qualitative results of BDBM on a test set of Edges \leftrightarrow Shoes.

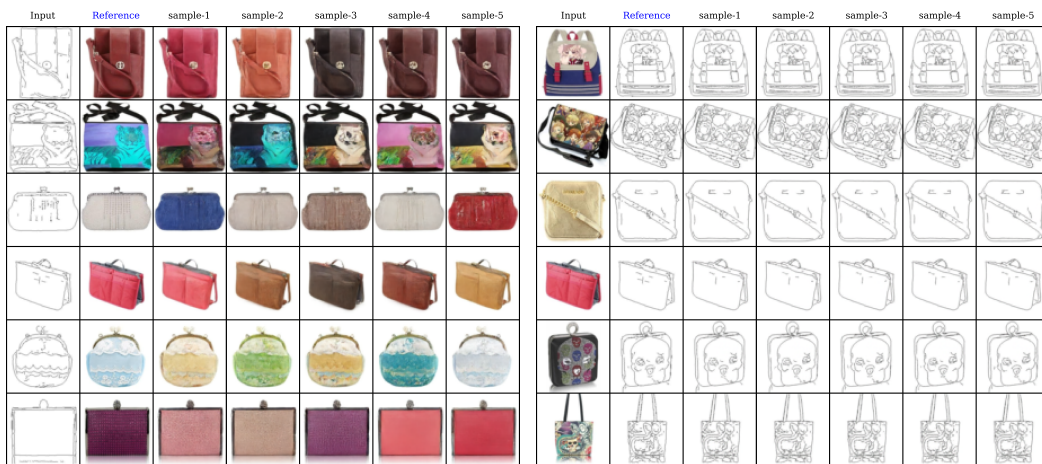


Figure 7: Qualitative results of BDBM on a test set of Edges \leftrightarrow Handbag.

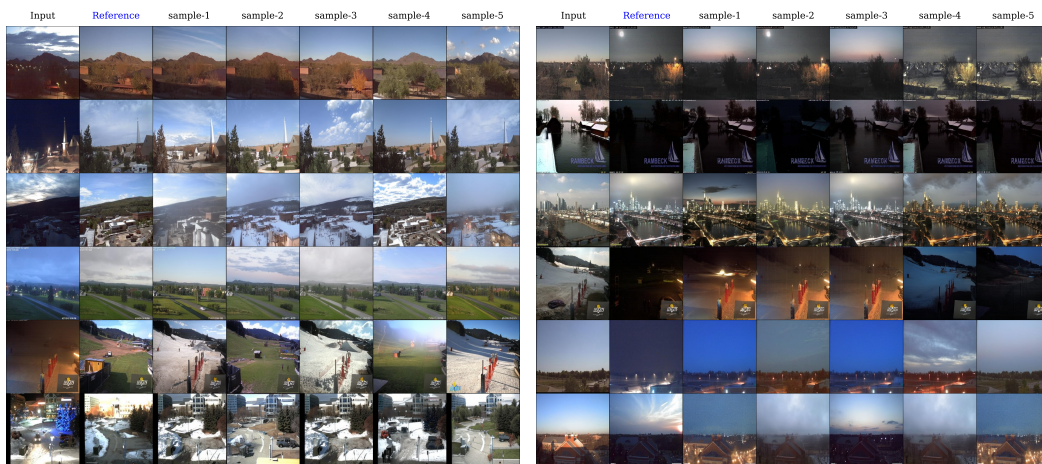


Figure 8: Qualitative results of BDBM on a test set of Night \leftrightarrow Day.

| Model | Shoes→Edges×64 | | | Handbags→Edges×64 | | | Outdoor→Normal×256 | | |
|-------------------|----------------|-------------|--------------|-------------------|-------------|--------------|--------------------|-------------|--------------|
| | FID ↓ | IS ↑ | LPIPS ↓ | FID ↓ | IS ↑ | LPIPS ↓ | FID ↓ | IS ↑ | LPIPS ↓ |
| BBDM | 0.66 | 2.23 | 0.006 | <u>1.54</u> | 3.11 | 0.010 | 18.87 | 5.82 | 0.122 |
| I ² SB | 1.02 | 2.14 | 0.015 | 1.98 | 3.08 | 0.018 | <u>11.54</u> | 5.97 | 0.229 |
| DDBM | 4.57 | 2.09 | 0.016 | 2.06 | 3.05 | 0.023 | 13.89 | <u>6.15</u> | 0.237 |
| BDBM-1 | <u>0.71</u> | <u>2.22</u> | <u>0.007</u> | 1.51 | <u>3.10</u> | <u>0.011</u> | 9.88 | 5.98 | 0.054 |
| BDBM | 0.98 | 2.20 | 0.009 | 1.87 | <u>3.10</u> | 0.016 | 11.69 | 6.27 | <u>0.069</u> |

Table 7: Results of BDBM and unidirectional baselines for the color-to-sketch and normal map translation tasks. The best results are highlighted in bold, while the second-best results are underlined.

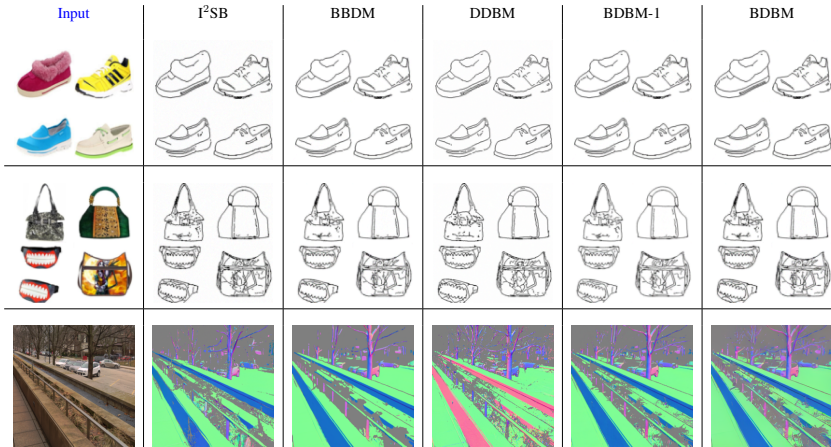


Figure 9: Samples generated by BDBM and unidirectional baselines for color-to-sketch/normal map translation.

B.2 Unidirectional translation from color images to sketch/normal maps

We further compare BDBM with unidirectional baselines BBDM, I²SB, DDBM, and BDBM-1 for color-to-sketch/normal map translation. For the baselines, we trained new models using the same settings as described in Section 4.1.2 for this translation direction, while for BDBM, we reused the checkpoints from Section 4.2.1 without retraining.

As shown in Table 7, BDBM performs comparably to most baselines and even surpasses some on specific datasets, despite using only *half* of the training resources. Notably, BDBM significantly outperforms DDBM and BBDM on the Shoes→Edges and Outdoor→Normal datasets, respectively, highlighting the computational efficiency of BDBM.

Qualitative differences between methods, however, are less apparent, as illustrated in Fig. 9. This is likely because sketches and normal maps contain fewer details than color images, making the metrics *more sensitive* to minor variations even when the generated images are visually similar to the targets.

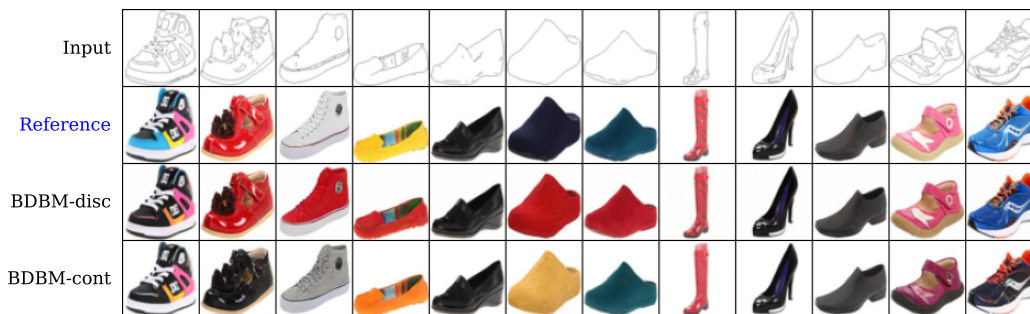
B.3 Continuous-time BDBM vs. Discrete-time BDBM

In this section, we compare discrete-time BDBM with its continuous-time counterpart. Both models are evaluated under identical settings, except that the continuous-time model allows t to take any real value in $[0, 1]$, while the discrete-time model restricts t to integer values in $[0, 1000]$.

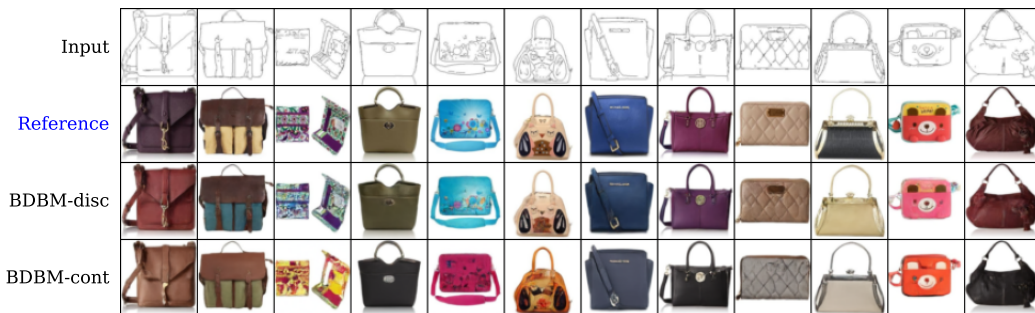
As shown in Table 8 and Fig. 10, discrete-time BDBM consistently outperforms its continuous-time counterpart. The primary reason for this advantage is that discrete-time BDBM only needs to predict noise for a fixed set of time steps, whereas the continuous-time model must handle an infinite number

| Model | Time type | Edges \leftrightarrow Shoes \times 64 | | Edges \leftrightarrow Handbags \times 64 | |
|--------|-----------------|---|--------------------|--|--------------------|
| | | FID \downarrow | LPIPS \downarrow | FID \downarrow | LPIPS \downarrow |
| BDBM-1 | discrete-time | 0.71/1.78 | 0.01/0.07 | 1.51/3.83 | 0.01/0.11 |
| | continuous-time | 1.28/1.81 | 0.01/0.03 | 2.45/3.94 | 0.02/0.17 |
| BDBM | discrete-time | 0.98/1.06 | 0.01/0.02 | 1.87/3.06 | 0.02/0.08 |
| | continuous-time | 2.38/2.41 | 0.01/0.04 | 2.88/3.79 | 0.04/0.16 |

Table 8: Comparison between discrete-time BDBM and continuous-time BDBM.



(a) Comparison between discrete-time BDBM and continuous-time BDBM on Edges \rightarrow Shoes \times 64.



(b) Comparison between discrete-time BDBM and continuous-time BDBM on Edges \rightarrow Handbags \times 64.

Figure 10: Visualization of discrete-time BDBM and continuous-time BDBM across Edges \rightarrow Shoes \times 64 and Edges \rightarrow Handbags \times 64. The first row shows the input images, the second row presents the ground truth images, while the third and fourth rows display the outputs of discrete-time and continuous-time BDBM, respectively.

of time steps. As a result, given the same number of training iterations, discrete-time BDBM can allocate more iterations to refining noise prediction at each specific time step, leading to more accurate predictions. This highlights the advantage of the discrete-time model when training iterations are limited. However, we anticipate that with a sufficient number of training iterations (as used for training continuous-time diffusion models [44]), both models would likely achieve comparable results.

B.4 More visualization on generated samples by BDBM

We provide additional qualitative translation results for Edges \rightarrow Shoes \times 64, Edges \rightarrow Handbags \times 64, and DIODE Outdoor \times 256, in Figs. 11, 12, and 13, respectively.

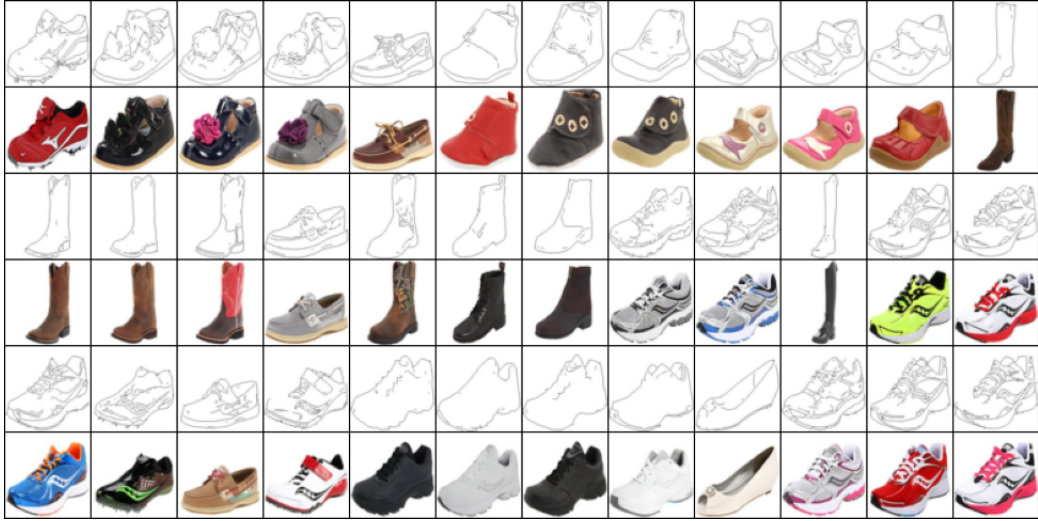


Figure 11: Additional qualitative results for Edges→Shoes×64, where each pair of consecutive rows displaying the input image in the “Edges” domain and its translation in the “Shoes” domain, respectively.

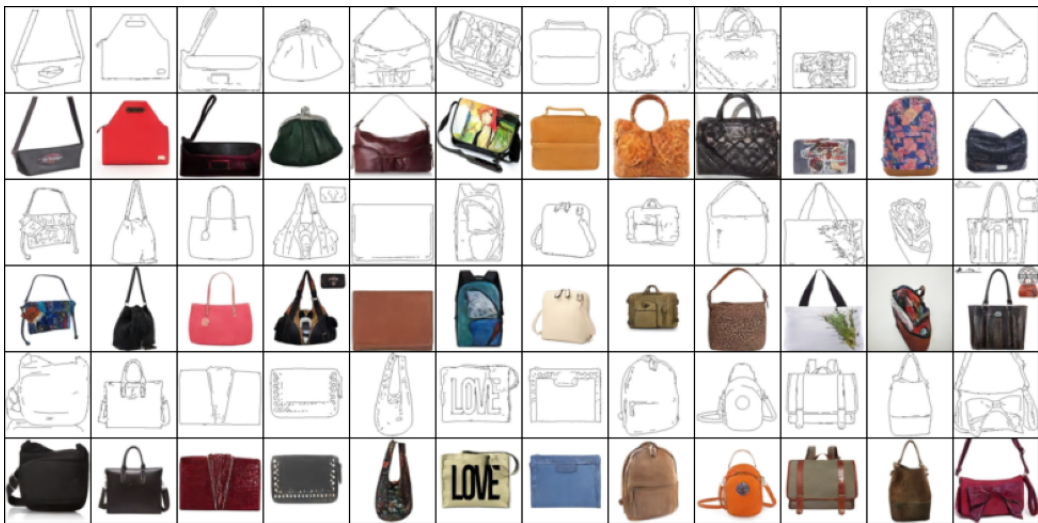


Figure 12: Additional qualitative results for Edges→Handbags×64, where each pair of consecutive rows displaying the input image in the “Edges” domain and its translation in the “Handbags” domain, respectively.



Figure 13: Additional qualitative results for DIODE Outdoor \times 256, where each pair of consecutive rows displaying the input image in the “Normal maps” domain and its translation in the “Color images” domain, respectively.